AGU ADVANCING EARTH AND SPACE SCIENCE

Tectonics

RESEARCH ARTICLE
10.1029/2020TC006129

Key Points:
- Supercontinent Nuna was finally assembled via a "soft collision" between Australia and Laurentia at circa 1.60 Ga
- Subsequent to the collision, the Mount Isa Inlier experienced slow exhumation (< ~0.5 mm yr^{-1}), mainly between circa 1.55 and 1.45 Ga
- Late Mesoproterozoic (ca. 1.55 Ga) postorogenic exhumation in the Mount Isa Inlier may have been associated with orogenic collapse

Supporting Information:
- Supporting Information S1
- Table S1
- Table S2

Correspondence to:
J. Li,
jiangyu.li@postgrad.curtin.edu.au

Citation:
Li, J., Pourteau, A., Li, Z.-X., Jourdan, F., Nordsvan, A. R., Collins, W. J., & Volante, S. (2020). Heterogeneous exhumation of the Mount Isa orogen in NE Australia after 1.6 Ga Nuna assembly: New high-precision $^{40}Ar/^{39}Ar$ thermochronological constraints. *Tectonics*, *39*, e2020TC006129. https://doi.org/10.1029/2020TC006129

Received 13 FEB 2020
Accepted 23 OCT 2020
Accepted article online 3 NOV 2020

Heterogeneous Exhumation of the Mount Isa Orogen in NE Australia After 1.6 Ga Nuna Assembly: New High-Precision $^{40}Ar/^{39}Ar$ Thermochronological Constraints

Jiangyu Li[1], Amaury Pourteau[1], Zheng-Xiang Li[1], Fred Jourdan[2], Adam R. Nordsvan[1,3], William J. Collins[1], and Silvia Volante[1,4]

[1]Earth Dynamics Research Group, ARC Centre of Excellence in Core to Crust Fluid Systems (CCFS), and The Institute for Geoscience Research (TIGeR), School of Earth and Planetary Sciences, Curtin University, Perth, Western Australia, Australia, [2]Western Australian Argon Isotope Facility, The Institute for Geoscience Research (TIGeR), School of Earth and Planetary Sciences, Curtin University, Perth, Western Australia, Australia, [3]Department of Earth Sciences, University of Hong Kong, Hong Kong, [4]Institute of Geology, Mineralogy and Geophysics, Ruhr-Universität Bochum, Bochum, Germany

Abstract The circa 1.60 Ga Isan Orogeny in NE Australia has been ascribed to the collision of Australia and Laurentia (North America), marking the final assembly of the Proterozoic supercontinent Nuna. However, details regarding the tectonic evolution of the orogen remain poorly constrained. To investigate the late orogenic to postorogenic thermal evolution and exhumation history, $^{40}Ar/^{39}Ar$ dating on hornblende, muscovite, and biotite was conducted in the Mount Isa Inlier, NE Australia, where intense crustal imbrication occurred during the Proterozoic continental collision. Published thermochronological results were recalculated using the current decay constant. Petrological examination and calculation of sample-specific $^{40}Ar/^{39}Ar$ closure temperatures and cooling rates were used to reconstruct the pressure-temperature evolution of individual structural domains. Diachronous cooling histories are revealed between western, central, and eastern belts through ~525–330°C, mainly between 1.53 and 1.48 Ga. Contrasting cooling across postmetamorphic fault zones records the reactivation of inherited normal (i.e., early basinal) and reverse (i.e., orogenic) faults. Estimated exhumation rates are generally low (< ~0.5 mm yr^{-1}), pointing to a modest local relief of < ~1,000 m which is comparable to modern analogs, and suggest a "soft" collision with limited crust thickening. Exhumation shortly following orogenesis was contemporaneous with felsic magmatism (1.55–1.48 Ga) in the eastern belt. Magmatism transitioning from trondhjemitic to A-type granitoids over this period suggests progressive heating of the orogen base, ascribed to lower crust delamination. Thus, thermochronological data reveal a regionally heterogeneous exhumation history controlled by orogenic collapse-related extensional faulting following the final assembly of the supercontinent Nuna.

1. Introduction

Despite the period of global orogenesis between circa 2.10 and 1.80 Ga, the supercontinent Nuna (also known as Columbia; Evans & Mitchell, 2011; Evans et al., 2016; Rogers & Santosh, 2002; Zhang et al., 2012; Zhao et al., 2002) was not completely assembled until the juxtaposition between Australia with Laurentia (North America) at circa 1.60 Ga (Figure 1a) (Betts et al., 2016; Kirscher et al., 2019, 2020; Nordsvan, Collins, Li, Spencer, et al., 2018; Pehrsson et al., 2016; Pisarevsky et al., 2014). In western Laurentia, this final Nuna amalgamation event was recorded by the Racklan and Forward orogenies (Furlanetto et al., 2013; Thorkelson et al., 2005), whereas in northeast Australia coeval orogenesis was recorded by the Isan and Jana orogenies of the Mount Isa and Georgetown inliers (Figure 1b), respectively (Betts et al., 2008; Pourteau et al., 2018; Volante, Collins, et al., 2020; Volante, Pourteau, et al., 2020; Withnall & Hutton, 2013).

In the Mount Isa Inlier (Figure 1), the Isan Orogeny resulted in large-scale crustal imbrication and regional metamorphism mainly along high thermobaric gradients (Abu Sharib & Sanislav, 2013; Bell & Rubenach, 1983; MacCready, 2006; Page & Bell, 1986), atypical of modern-style continental collision. Although it is generally thought that supercontinent amalgamation involves large-scale orogenesis

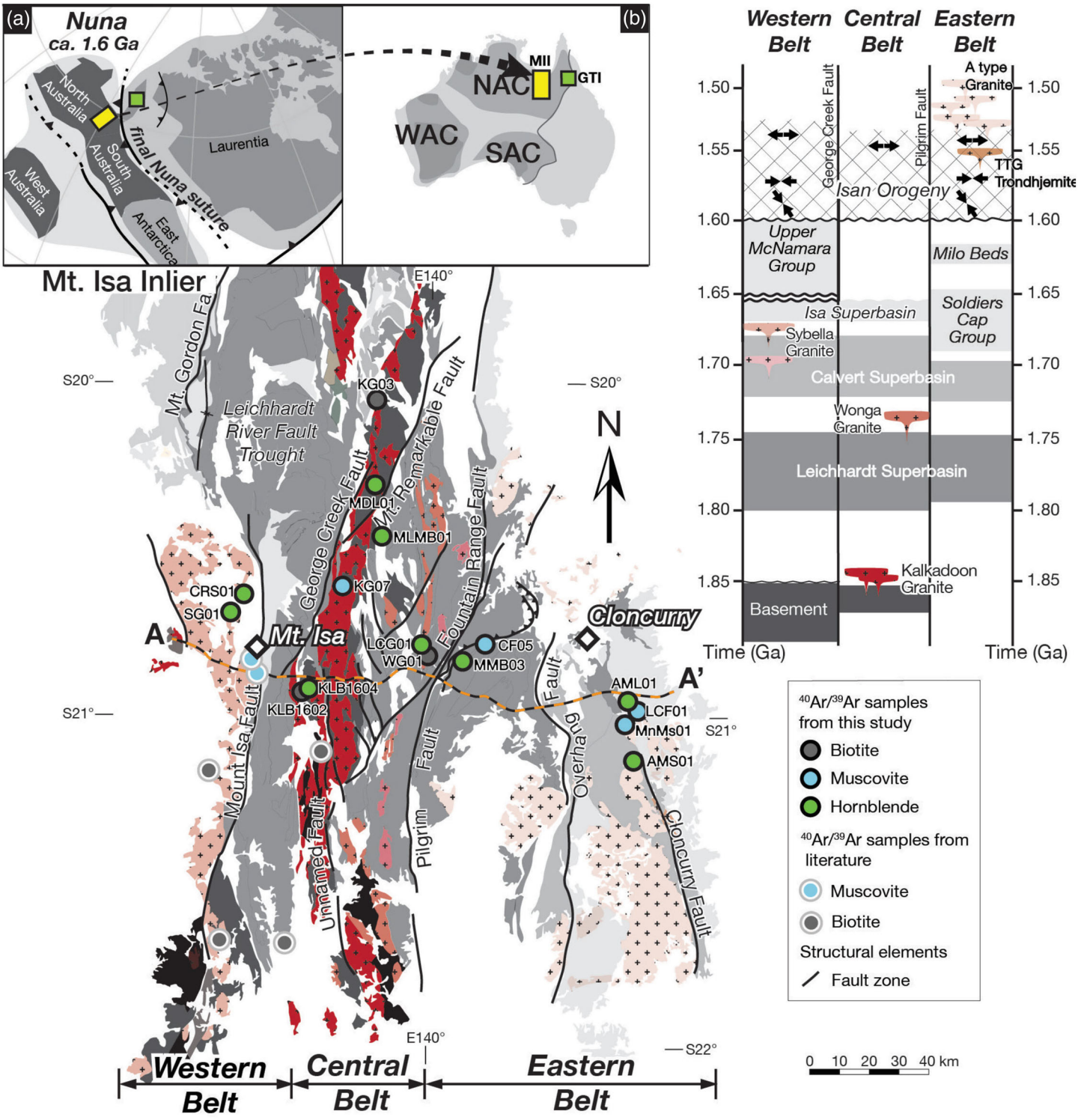

Figure 1. Simplified lithological map of the Mount Isa Inlier showing the successive stratigraphic packages (or "superbasins"), the main fault zones, $^{40}Ar/^{39}Ar$ sample locations from this study and selective results from literature (relative selective criteria are described in section 3.2.). Transect A-A′ shows the trace of Geoscience Australia geophysical imaging profile 94MTI-1. Inset a: Paleogeography reconstruction of the NE Australia at circa 1.60 Ga (Pourteau et al., 2018) showing the inferred location of the study area (yellow box) and Georgetown Inlier (green box) along the final Nuna suture zone. Inset b: Location of the study area to the Australian cratons. NAC, North Australian Craton; WAC, West Australian Craton; SAC, South Australian Craton, MII, Mount Isa Inlier; GTI, Georgetown Inlier.

representing the closure of wide oceans (Brown, 2007; Johnson et al., 2012), collisional processes prevalent during the Isan Orogeny remain cryptic due to a general paucity of diagnostic plate boundary features such as (1) exposed ophiolites or accretionary complexes, (2) precollisional arc magmatism, and (3) high-pressure metamorphic rocks reflecting significant crustal thickening (Foster & Rubenach, 2006; Pourteau et al., 2018). Nevertheless, recent investigations of sedimentary provenance (Nordsvan, Collins, Li, Spencer, et al., 2018) and metamorphic record (Pourteau et al., 2018) suggest that the Georgetown Inlier of NE Australia might represent part of an allochthonous terrane that collided with the North Australia Craton during the Isan Orogeny. The exact nature of this collisional event remains ambiguous.

Understanding tectonic processes during continental collision requires detailed knowledge of the timing and duration of the associated deformation, metamorphism, and crustal exhumation (Johnson et al., 2012; Kearey et al., 2009). Isotopically derived thermal histories partly record the denudation of an uplifted region and provide insights into orogenic and crustal evolution processes as they constrain the activity of crustal faults (McDougall & Harrison, 1999; Skipton et al., 2017; Stübner et al., 2018). In this study, high-precision $^{40}Ar/^{39}Ar$ thermochronology from igneous and metamorphic rocks from the Mount Isa Inlier are used to decipher the cooling history associated with the Isan Orogeny. Sampling was conducted along an E-W corridor (Transect A-A′ in Figure 1) across different crustal domains of the inlier. Geochronology results, combined with the metamorphic and magmatic records, are used to reconstruct and compare the cooling history across different crustal domains, infer the kinematics of postorogenic faulting, and discuss the driving mechanism for the postorogenic crustal exhumation.

2. Geological Setting

2.1. Regional Geology

The Mount Isa Inlier of NE Australia consists of high-grade metamorphic and crystalline basement rocks (the >1.85 Ga Kalkadoon-Leichhardt Complex; Blake, 1987; Etheridge et al., 1987) that are overlain by three successive superbasins including the circa 1.8–1.74 Ga Leichhardt Superbasin, the circa 1.73–1.69 Ga Calvert Superbasin, and the circa 1.67–1.58 Ga Isa Superbasin (Betts et al., 2006; Blake, 1987; Foster & Austin, 2008; Jackson et al., 2000; Neumann et al., 2006). The Inlier has been subjected to polyphase shortening, widespread, generally low-pressure metamorphism, and synorogenic to postorogenic magmatism at circa 1.60–1.50 Ga (Abu Sharib & Sanislav, 2013; Betts, 1999; Mark, 2001; Page, 1983; Reinhardt, 1992b; Sayab, 2006, 2009; Wyborn, 1998). These events were collectively ascribed to the Isan Orogeny, marking the collision between NE Australia and NW Laurentia (Betts et al., 2006; Furlanetto et al., 2013; Gibson et al., 2018; Pourteau et al., 2018). Although the Mount Isa Inlier has been subdivided into 15 fault bound domains (Withnall & Hutton, 2013, 11 of them are shown in Figure 2) based on their discrete sedimentary records and geophysical characters; for simplicity, it can also be divided into three major belts (Day et al., 1983) (Figure 1) that are separated by major N-S to NE-SW major faults: the western belt, west of the George Creek, and Mount Isa faults; the eastern belt, east of the Fountain Range, and Pilgrim faults; and the intervening central belt.

In the western belt, the Leichhardt Superbasin siliciclastic and mafic volcanic rocks formed in a N-S striking rift (Jackson et al., 2000; O'Dea, Lister, Betts, & Pound, 1997) that were subsequently folded circa 1.73 Ga (Blaikie et al., 2017; Jackson et al., 2000). Locally, these rocks are overlain by bimodal volcanics and fluvial to shallow-marine sedimentary rocks of the Calvert Superbasin (Derrick, 1982; Gibson et al., 2008; Jackson & Southgate, 2000; O'Dea, Lister, Betts, & Pound, 1997), which are in turn overlain by the circa 1.67–1.59 Ga carbonaceous and clastic sandstones of the Isa Superbasin (Betts et al., 1998; Betts & Lister, 2001; Southgate et al., 2000). The circa 1.66 Ga Sybella batholith intruded the basement and the Leichardt succession in the Sybella Domain at shallow crustal levels (Connors & Page, 1995; Gibson et al., 2008; Page & Bell, 1986), causing contact metamorphism that locally reached amphibolite facies (Blenkinsop, 2005). The Mount Isa fault zone, which separates the Sybella and Leichhardt River domains, marks a significant metamorphic gap, with generally greenschist-facies rocks to the east and amphibolite-facies rocks to the west (Foster & Rubenach, 2006; Rubenach, 1992). Regional metamorphism along the western flank of the Mount Isa fault zone was dated with garnet Nd-Sm at circa 1575 Ma (Duncan et al., 2006; Hand & Rubatto, 2002).

In the central belt, the oldest formation overlying the Kalkadoon-Leichhardt Complex consists of circa 1.79 Ga bimodal volcanic rocks exposed along the eastern margin of a basement horst

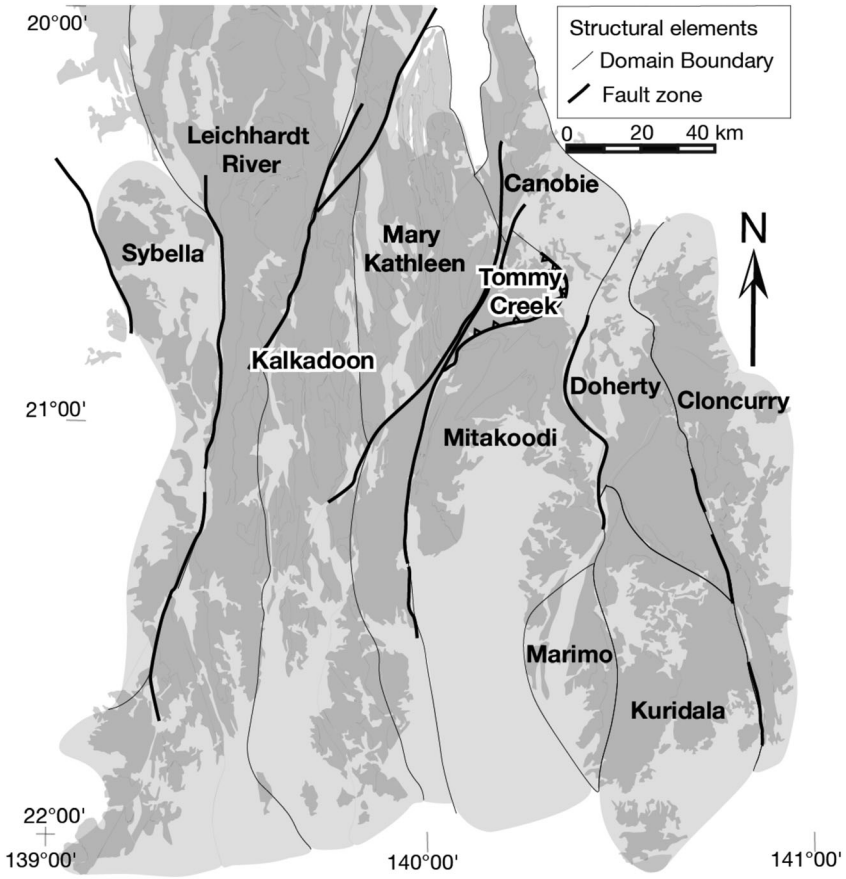

Figure 2. Geological domains of the Mount Isa Inlier (Withnall & Hutton, 2013) separating by geophysical boundaries or major faults. Dark gray regions are exposed Proterozoic rock of the Mount Isa Inlier, and light gray is under cover.

(Jackson et al., 2000). Associated with NW-SE extension, the graben was filled with Leichhardt Superbasin siliciclastic fluvial to shallow marine sediments (Eriksson et al., 1994; Jackson et al., 2000; Neumann et al., 2009) and is overlain locally by Calvert Superbasin shallow marine sandstones and Isa Superbasin dolomitic sandstones (Jackson et al., 2000; Page et al., 1997). At circa 1.74–1.73 Ga, the granitic Wonga suite (with subordinate gabbro) intruded the eastern central belt along a N-S midcrustal detachment zone (Gibson et al., 2008; Holcombe et al., 1991; Oliver et al., 1991; Pearson, 1992). Amphibolite facies contact metamorphism occurred under an elevated thermal regime during granite intrusion (Oliver et al., 1991), and such metamorphic rocks were tightly folded during the Isan Orogeny (Bell et al., 1992). Isan metamorphism in the central belt was generally in upper greenschist facies but culminated in upper amphibolite facies in the Mary Kathleen Domain at circa 1.57 Ga (Foster, 2003; Foster & Rubenach, 2006; Hand & Rubatto, 2002; Reinhardt, 1992a).

In the eastern belt, the oldest formation of the Leichhardt Superbasin succession contains circa 1.76–1.74 Ga bimodal felsic and mafic volcanics, sandstone, and carbonate rocks (Beardsmore et al., 1988; Foster & Austin, 2008; Jackson & Southgate, 2000; Page, 1998; Page & Sun, 1998) and was locally intruded by circa 1.75–1.74 Ga granites in the Marimo Domain (Page & Sun, 1998). The Leichhardt succession was overlain by Calvert shallow-marine sedimentary rocks in the Doherty Domain (Gibson et al., 2012; Southgate et al., 2013) and, further east, by circa 1.68–1.66 Ga quartzite, and basalt of the Soldiers Cap Group in the Cloncurry Domain, considered part of the Isan Superbasin (Foster & Austin, 2008; Page & Sun, 1998). The metamorphic grade varies across major faults and within individual domains (Foster & Rubenach, 2006; Sayab, 2006). Bound to the east by the subvertical Cloncurry fault, the Cloncurry Domain, which is the eastmost domain of the Mount Isa Inlier, exhibits greenschist to upper amphibolite facies metamorphic assemblages, with prograde garnet formed at circa 1.60 Ga (Pourteau et al., 2018) and

peak monazite at circa 1.59–1.58 Ga (Giles & Nutman, 2002; Hand & Rubatto, 2002). West of the Cloncurry fault, the metamorphism grade only reached lower greenschist facies in the Doherty and Mitakoodi domains (Foster & Rubenach, 2006). Following the metamorphism and most of the deformation, the eastern belt was intruded by a minor circa 1.55 Ga trondhjemite pluton (Mark, 2001; Page & Sun, 1998) near the Cloncurry fault and by voluminous circa 1.54–1.49 Ga A-type granite plutons of the Williams and Naraku batholiths (Mark, 2001; Pollard et al., 1998; Wyborn, 1998).

2.2. Orogenic Evolution

Although the kinematic evolution of the Isan Orogeny is complex and controversial (Betts et al., 2006; Connors & Lister, 1995; Giles et al., 2006; O'Dea, Lister, Maccready, et al., 1997; O'Dea & Lister, 1995), most studies suggest that the orogeny is polyphased and initiated at circa 1.60 Ga with N-S crustal shortening in the western belt, reversing early E-W trending normal basinal faults (Bell, 1983, 1991; Bell et al., 1992; Betts et al., 2006; Blake, 1987; Lister et al., 1999; O'Dea & Lister, 1995; O'Dea, Lister, Betts, & Pound, 1997). This early Isan orogenic phase was coeval with NW directed folding and thrusting along mylonitic detachments in the eastern belt, with thin-skinned nappe stacking developed at low- to medium-P/T conditions (Betts et al., 2006; MacCready, 2006; O'Dea et al., 2006). Continuous deformation evolved into thick-skinned, E-W shortening, producing N-S striking basement-rooted reverse faults and upright to steeply inclined folds at all scales (Betts et al., 2000; Blenkinsop et al., 2008; MacCready, 2006; MacCready et al., 1998; O'Dea et al., 2006). Although early geochronological studies suggested that the dominant E-W shortening event occurred circa 1.55–1.53 Ga (Connors & Page, 1995; Foster & Rubenach, 2000; Page, 1983; Pollard & Perkins, 1997; Rubenach & Barker, 1998), more recent studies indicate that the metamorphism associated with the deformation occurred circa 1.60–1.58 Ga (Abu Sharib & Sanislav, 2013; Duncan et al., 2006; Foster & Rubenach, 2006; Gauthier et al., 2001; Giles & Nutman, 2002; Hand & Rubatto, 2002; Pourteau et al., 2018). Following the Isan Orogeny, the regional deformation was interpreted to be transpressional at a wrenching stage (Lister et al., 1999; O'Dea, Lister, Maccready, et al., 1997), with crustal shortening accommodated by conjugate NW striking sinistral and NE striking dextral faults along inherited early normal faults (Lister et al., 1999). The activity of these faults has not been precisely dated, but it certainly represents a postorogenic deformational phase (Betts et al., 2006; Williams & Phillips, 1992).

3. Previous Thermochronology Results

3.1. State of the Art

Several geochronological studies have previously tackled the thermal history of the Mount Isa Inlier (Perkins & Wyborn, 1998; Richards et al., 1963; Spikings et al., 2001, 2002). Cooling age populations of ~1.77 Ga from the western belt and 1.45–1.40 Ga from the central belt, obtained via the K/Ar method on biotite and muscovite from circa 1.86–1.67 Ga granitoids, were ascribed to an Isan Orogeny-related thermal event that affected only the central belt, which marked a "metamorphic discontinuity" across the George Creek boundary fault (Richards et al., 1963). Given the analytical limitations of the K/Ar method (Kelley, 2002), subsequent studies applied the $^{40}Ar/^{39}Ar$ method on K-bearing minerals across the inlier (Perkins & Wyborn, 1998; Pollard & Perkins, 1997; Spikings et al., 2001, 2002). Hornblende and muscovite $^{40}Ar/^{39}Ar$ ages from igneous and metamorphic rocks showed an early phase of cooling at 1.45–1.39 Ga, whereas biotite and K-feldspar revealed a later stage cooling at 1.28–1.0 Ga (Spikings et al., 2001, 2002). The early phase of cooling was correlated with exhumation and shearing in the Arunta Inlier of central Australia and the Gawler Craton in South Australia. The later phase of cooling was interpreted to record thermal relaxation after the intrusion of ~1.11 Ga dolerite dykes in the central belt of the Mount Isa Inlier (Spikings et al., 2002). Hydrothermal hornblende and biotite associated with copper mineralization were dated using the $^{40}Ar/^{39}Ar$ method and yielded a consistent age of circa 1.53 Ga for both the western and eastern belts (Baker et al., 2001; Perkins et al., 1999). Synkinematic muscovite from the Cloncurry fault (eastern belt) and the Mount Isa fault zone (10 km southwest of the Mount Isa town) was dated at circa 1.51 Ga (Baker et al., 2001) and circa 1.40 Ga (Perkins et al., 1999), respectively. The youngest cooling event was dated by apatite fission-track thermochronology (i.e., below ~120°C) at circa 0.39 and 0.23 Ga and is thought to be associated with far-field effects of orogenic events in central or eastern Australia (Spikings et al., 1997).

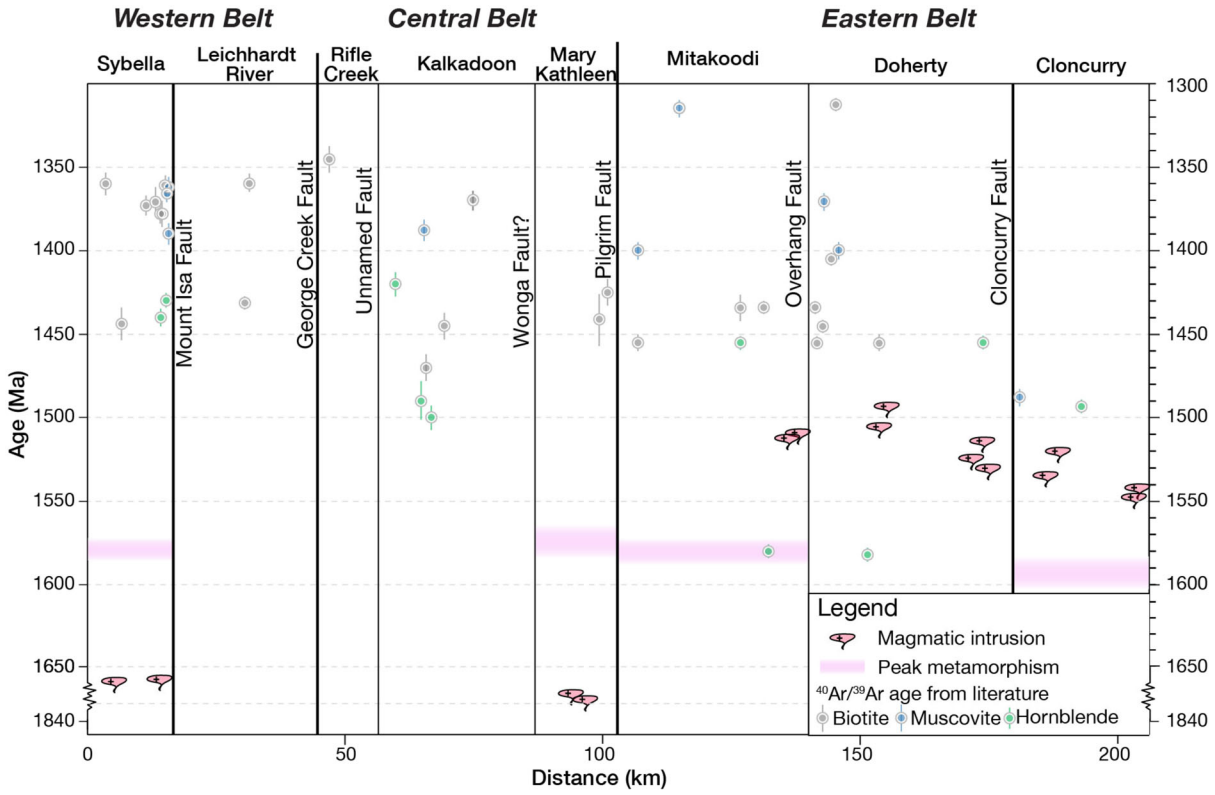

Figure 3. Time versus distance plot of previously published $^{40}Ar/^{39}Ar$ ages along a W-E transect across the Mount Isa Inlier (Line A-A′ in Figure 1) (Perkins & Wyborn, 1998; Pollard & Perkins, 1997; Spikings et al., 2001, 2002).

3.2. Reassessment of Available $^{40}Ar/^{39}Ar$ Data

Crustal cooling within the Mount Isa inlier has been the subject of numerous studies and is fundamental to our understanding of the Proterozoic crustal evolution of NE Australia. However, after plotting existing $^{40}Ar/^{39}Ar$ ages along an E-W transect across the Mount Isa Inlier (Figure 3), an apparent age gap of ~140 Myr appears between peak metamorphism (at ca. 1.59 Ga) and the subsequent cooling event (mainly from ca. 1.45 Ga), and some ages contradict with each other. For example, hornblende with a high closure temperature ($Tc \approx 500$°C; Harrison, 1981) yielded younger dates than biotite ($T \approx 310$°C; Harrison et al., 1985) in places such as the Kalkadoon Domain (ca. 1453 Ma biotite vs. ca. 1419 Ma hornblende). Individual structural domains yielded heterogeneous $^{40}Ar/^{39}Ar$ ages for the same mineral, for example, biotite from the Sybella Domain yielding a range of dates between 1.12 and 1.44 Ga (Figure 3). Thus, after carefully examining the published $^{40}Ar/^{39}Ar$ ages, it appears that various causes may have hindered the quality, and hence the geological significance, of a large proportion of previous $^{40}Ar/^{39}Ar$ data. These include (i) heterogeneous, partial resetting of the argon isotopic system of the dated samples (see Warren et al., 2012), (ii) multiple argon diffusion domains leading to argon loss due to mineral lattice defects (through, e.g., dissolution or exsolution; McDougall & Harrison, 1999), and (iii) radiogenic argon released from preexisting muscovite being trapped in the newly generated muscovite within the same rock, causing the excess argon effect (McDonald et al., 2018).

To reevaluate previous thermochronological results, the published data were recalculated using an updated argon decay constant of 0.576 ± 0.002 E-10 1/a (Renne et al., 2011). We then graded the quality of each data set based on their argon release percentage and mini plateau stages (Table S1 in the supporting information) following the criteria of Hansma et al. (2016). An accepted plateau age should have a low scatter with a p value > 0.05 and encompass at least 70% of ^{39}Ar released (or 50% for an acceptable but less reliable age) with miniplateaus over a minimum of three consecutive steps agreeing at 95% confidence level (Hansma et al., 2016).

4. Methodology

4.1. Sample Strategy and Petrology

Sixteen samples were collected from an E-W transect aligned with the deep-seismic profile (Figure 1: 94MTI-01; Geoscience Australia). Samples taken closest to the transect are for investigating E-W variations in the cooling record, whereas samples to the north or south of the profile are for detecting possible lateral variations within each domain. The sampling was optimized to better understand the timing, kinematics, and magnitudes of fault movement along major fault zones and to compare the evolution of the crustal zones with various metamorphic grades. Detailed petrographic features are described in section 5.1, whereas the sampled outcrop and thin section photos are provided in Figures S7–S9 of the supporting information.

4.2. Closure Temperature of Dated Minerals

To calculate the closure temperature of different mineral grains, we use the activation energy, diffusion coefficient, and volume constant of Harrison (1981) for hornblende, Harrison et al. (2009) for muscovite, and Grove and Harrison (1996) for biotite. Initial closure temperature value (T_{i_c}) refers to those published from argon diffusion experiments, that is, 500°C for hornblende (Harrison, 1981), 425°C for muscovite (Harrison et al., 2009), and 310°C for biotite (Harrison et al., 1985) at a cooling rate of 10°C/Ma. The effective diffusion radius (a) was based on the grain sizes of the dated mineral. Specific parameter values for calculating the closure temperature of each sample are listed in Table S3 of the supporting information. The initial cooling rates (dT/dt) are assessed from the peak metamorphic stage to the time of mineral's closure temperature (as defined by Dodson, 1973). Peak metamorphic ages are summarized from previous work (Gauthier et al., 2001; Hand & Rubatto, 2002; Pourteau et al., 2018; Rubenach et al., 2008) and listed in Table S2 of the supporting information. The peak temperature map (Figure 4) was modified from Foster and Rubenach (2006) and references therein.

4.3. Cooling Rate

Specific closure temperatures for hornblende, muscovite, and biotite were used to calculate cooling rates for different mineral pairs dated in this study within individual tectonic domains. In areas where closure temperature constraints for biotite are unavailable (e.g., the Sybella Domain), the closure temperatures from previous single-grain argon dating (Spikings et al., 2002) were recalculated and used. Published argon results were recalculated using the updated argon decay constant of Renne et al. (2011) and then selected following the criteria of Hansma et al. (2016) as defined in section 3.2. Individual age spectra are plotted in Figures S1–S4 of the supporting information. Nine previously reported ages were incorporated into Figures 5–7, with the calculated cooling rates listed in Table 1 and plotted in a time versus distance diagram (Figure 8). Uncertainties for the closure temperature and cooling rate calculations were estimated using Monte Carlo simulation. Detailed descriptions are summarized in Text S2 of the supporting information.

5. Results

5.1. Petrography

Sample descriptions are organized broadly from west to east in their respective domains. Outcrop and thin section photos are provided in the supporting information (Figures S7–S9). For the picking of the dated mineral grains, particular care was given to the petrology and mineralogy of the sample through microscopic examination. Samples with strong alteration and fluid influence were excluded, and the presence of secondary phases (e.g., chlorite) was carefully investigated.

5.1.1. Sybella Domain

Sample SG01 is a potassium-rich A-type granite collected from the Sybella Batholith, west of the Mount Isa fault zone (Figure 1). This rock mainly comprises quartz (30%), K-feldspar (~20%), plagioclase (~15%), biotite (~15%), amphibole (~10%), and accessory minerals including apatite (~5%) and zircon (~5%). The granite is medium to coarse-grained and characterized by centimeter-sized K-feldspar phenocrysts with albite or oligoclase rims (Figures S7A and S7a). The rock's foliation is defined by preferentially orientated amphibole, biotite, K-feldspar, and quartz-opaque aggregates. The penetrative foliation identified in the Sybella Granite is parallel to both intrusive margins and the fabric in the country rock.

Sample CRS01 is a foliated amphibolite of the May Downs Gneiss from the country rock of the Sybella Granite that was collected 5 km northeast of SG01. The sample comprises mainly amphibole

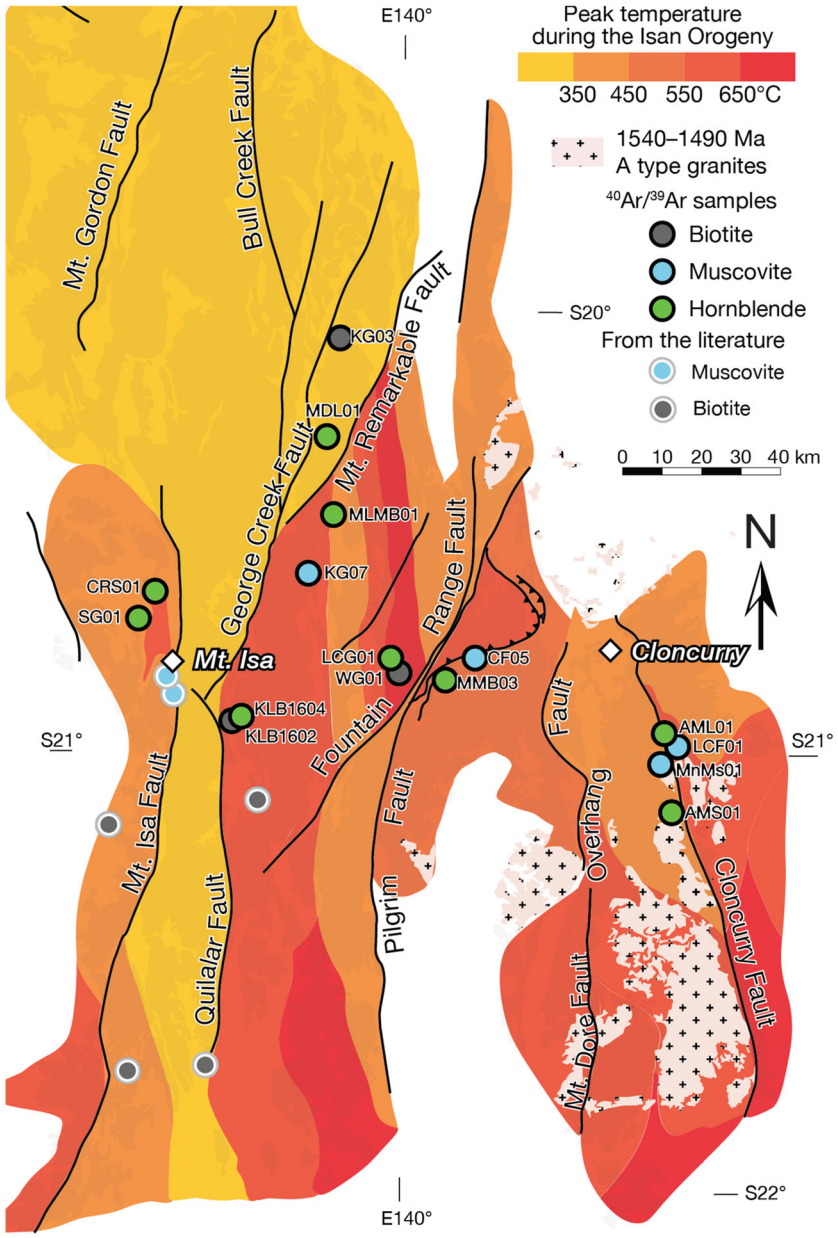

Figure 4. Peak temperature map of the Mount Isa Inlier during the Isan Orogeny at circa 1.59–1.57 Ga, modified from Foster and Rubenach (2006) after integrating estimated peak metamorphism temperature (Blenkinsop, 2005; Gauthier et al., 2001; Giles & Nutman, 2002; Hand & Rubatto, 2002; Page & Sun, 1998; Pourteau et al., 2018; Rubenach et al., 2008). Specific values of the metamorphism temperature in each domain are listed in Table S2 in the supporting information.

(~65%; vol%), plagioclase (~15%), quartz (~15%), and minor biotite (~5%). The pervasive L-tectonite fabric is defined by the preferred orientation of dark green amphibole, with aggregated plagioclase and quartz filled interstitially (Figure S7b). Locally, euhedral light green amphibole at a high angle to the matrix foliation suggests that it is postkinematic.

5.1.2. Kalkadoon Domain

Sample KLB1604 is an amphibolite collected from the Kurbayia Metamorphic Complex in the Kalkadoon Domain. The sample comprises mainly millimeter-sized brown amphibole (~60%), plagioclase (~35%), and minor quartz and ilmenite. Amphibole grains are subhedral and have straight contacts with plagioclase and quartz. Amphibole is commonly dark brown and dark green and forms a dominant granoblastic texture.

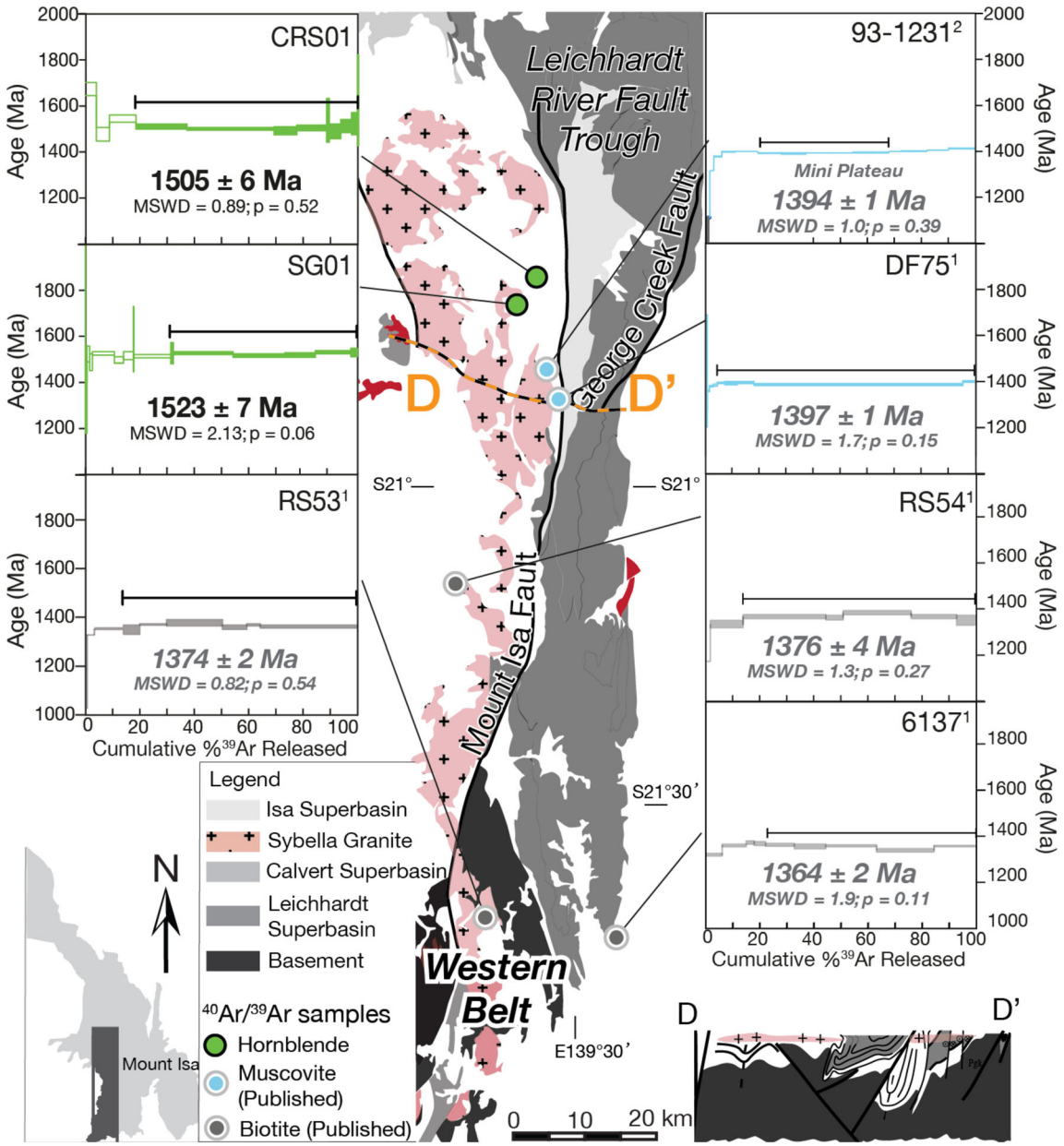

Figure 5. Simplified lithological map and cross section (modified after MacCready, 2006) of the western belt of the Mount Isa Inlier with sample locations and $^{40}Ar/^{39}Ar$ age spectra. Spectra with ages in light gray and italic are the $^{40}Ar/^{39}Ar$ results recalculated from the literature: 1 = Spikings et al. (2002) and 2 = Perkins et al. (1999). Spectra with ages in dark black and plateaus in green, blue, and dark gray are from this study.

Prismatic plagioclase crystals are primarily euhedral with minor grains displaying a more subhedral crystal form. Multiple twins are observed in most plagioclase crystals. Locally, overgrowth of light green amphibole rims around amphibole crystals and fine-grained aggregates of sericite (Figure S7c) suggest overprinting.

Sample KLB1602 is a biotite-bearing gneiss collected from the Kurbayia Metamorphic Complex, 0.5 km west of KLB1604. The sample comprises mainly quartz (~40%), biotite (~30%), muscovite (~10%), plagioclase (~10%), and accessory minerals such as apatite and zircon. The sample is strongly deformed, with a pervasive foliation defined by layers of orientated biotite alternating with quartz-feldspathic layers, suggests mineral growth synkinematic with the pervasive foliation.

Sample MLMB01 is a metabasalt (Figure S7D) collected from the Magna Lynn Metabasalt member, 10 km south of the Mount Remarkable fault (Figure 1). The sample is composed of oriented light green to dark

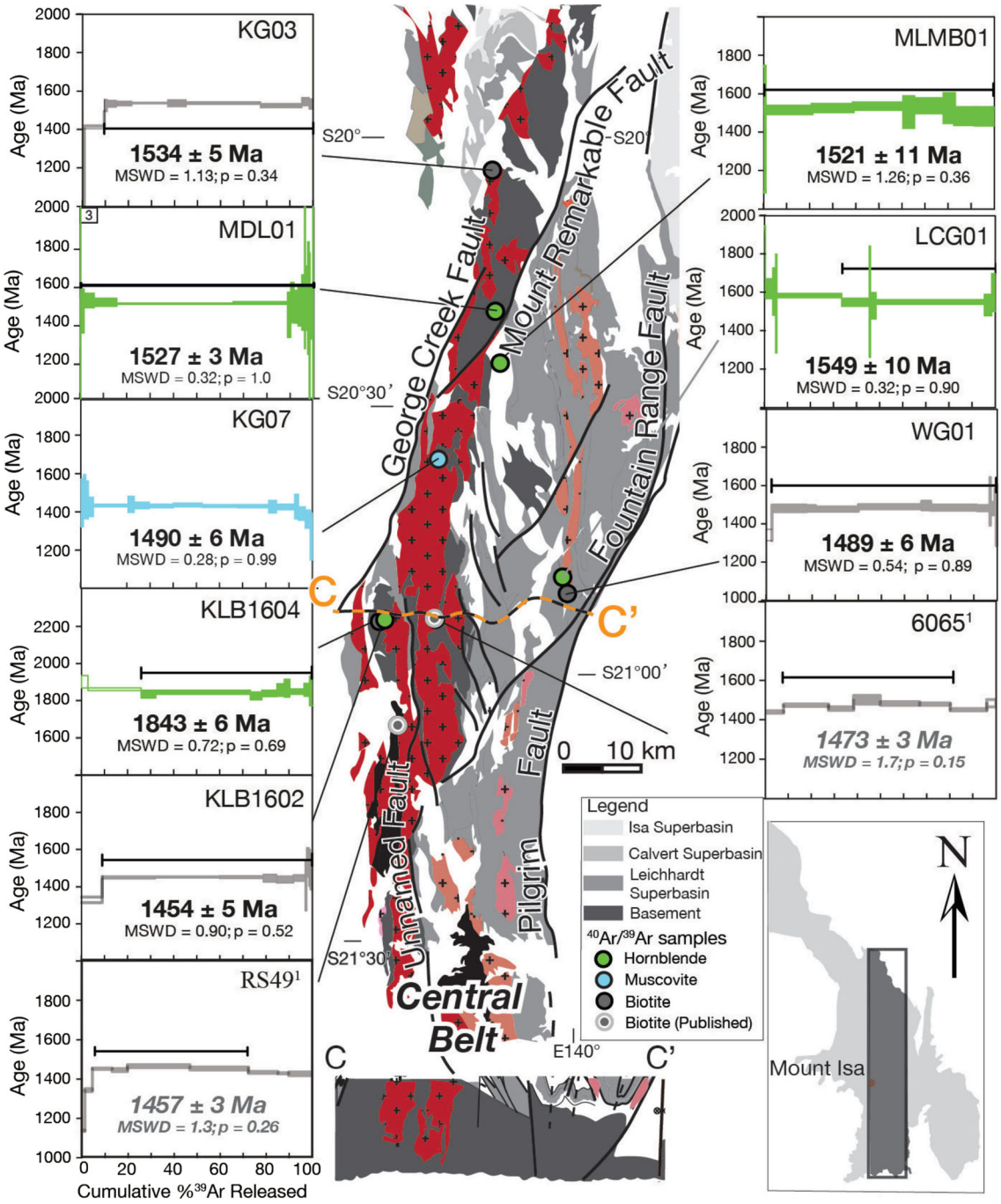

Figure 6. Simplified lithological map and cross section (modified after MacCready, 2006) of the central belt with sample locations and $^{40}Ar/^{39}Ar$ age spectra. Spectra with ages in light gray and italic are the $^{40}Ar/^{39}Ar$ results recalculated from the literature: 1 = Spikings et al. (2002). Spectra with ages in dark black and plateaus in green, blue, and dark gray are from this study.

blue prismatic phenocrysts of amphibole, defining the magmatic flow direction in the groundmass of very fine grained plagioclase quartz-amphibole-opaque (Figure S7d) and shows the primary igneous volcanic texture. The light green amphibole is slightly altered by chlorite (Figure 7d), suggesting a low-grade greenschist-facies metamorphic overprint.

Sample KG03 is a medium- to coarse-grained, biotite-bearing granite from the Kalkadoon Supersuite (Figure 1). The sample is a pinkish, massive granite (Figure S8A) with coarse quartz, plagioclase, and

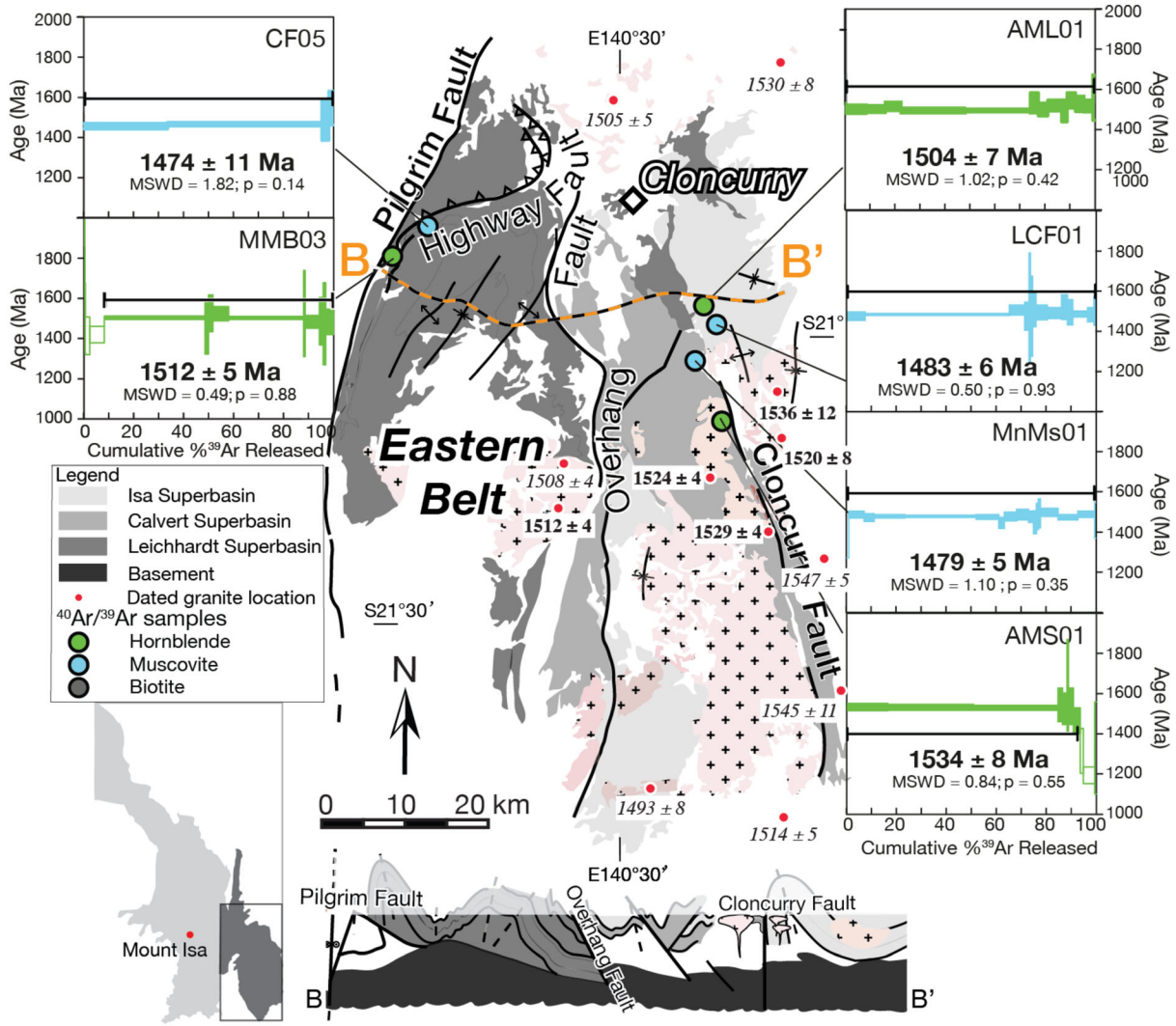

Figure 7. Simplified lithological map and cross section of the eastern belt of the Mount Isa Inlier (modified after MacCready, 2006) with $^{40}Ar/^{39}Ar$ age spectra and sample locations. Red dots represent the sample location of the circa 1550 to 1490 Ma granites dated from the literature: Ages in bold are from Pollard and McNaughton (1997), and ages in italic are from Page and Sun (1998).

K-feldspar phenocrysts, biotite, rare hornblende, and accessory minerals including zircon, apatite, and monazite. The sample retains its primary igneous texture, with small recrystallized subhedral quartz aggregates growing interstitially between primary igneous mineral phases (Figure S8a).

5.1.3. Mary Kathleen Domain

Sample LCG01 is a metagabbro collected from the Lunch Creek Gabbro, 15 km north of the Pilgrim fault. The sample is composed of plagioclase, amphibole, quartz, biotite, and minor pyroxene. Pyroxene is locally preserved but is mostly replaced by dark brown amphibole. Plagioclase is partially replaced by fine-grained aggregates of sericite, epidote, and minor chlorite (Figure S8b), while biotite is subhedral and partially replaced by prehnite. Quartz grew interstitially between plagioclase and amphibole grains.

Sample WG01 is a hornblende-biotite-bearing granite collected from the Wonga Suite, 3 km south of Sample LCG01. The sample is composed of quartz (45%), plagioclase (20%), biotite (15%), K-feldspar (5%), hornblende (5%), and accessory minerals including titanite and apatite (Figure S8c). The sample has a well-foliated augen texture, with biotite-rich layers wrapping porphyroblasts of quartz aggregates. The porphyroblastic quartz exhibits undulose extinction, and it shows annealing and grain boundary migration suggesting partial recrystallization.

Table 1
Cooling Rates Calculated From Mineral Pairs of Hornblende, Muscovite, and Biotite From Each Tectonic Domain at Specific Closure Temperatures

Domain	Cooling rate$^{I3}_{I1}$(°C/Ma)	Cooling period (Ma)	Mineral pair	Cooling temperature (°C ± 2 SD)
Eastern Belt				
Cloncurry Domain	$1.5^{+0.2}_{-1.2}$°C/Ma	1575–1503 Ma	Metamorphism-Hbl	575 ± 55 517 ± 52
	$5.9^{+4.8}_{-3.1}$°C/Ma	1503–1483 Ma	Hbl-Ms	517 ± 52 397 ± 48
(Average cooling rate)	$1.9^{+0.8}_{-0.3}$°C/Ma	1575–1483 Ma	Metamorphism-Ms	575 ± 55 397 ± 48
Doherty Domain	$2.1^{+1.1}_{-1.0}$°C/Ma	1534–1479 Ma	Hbl-Ms	526 ± 48 410 ± 50
Mitakoodi Domain	$2.1^{+1.7}_{-1.6}$°C/Ma	1511–1474 Ma	Hbl-Ms	486 ± 54 408 ± 50
Central belt				
Mary Kathleen Domain	$4.2^{+0.7}_{-2.1}$°C/Ma	1575–1549 Ma	Metamorphism-Hbl	590 ± 40 524 ± 48
Mary Kathleen Domain	$3.3^{+1.2}_{-1.1}$°C/Ma	1549–1489 Ma	Hbl-Bt	524 ± 48 328 ± 58
(Average cooling rate)	$3.7^{+1.0}_{-1.5}$°C/M	1575–1489 Ma	Metamorphism-Bt	590 ± 40 328 ± 58
Central Kalkadoon Domain	$2.6^{+1.5}_{-1.0}$°C/Ma	1521–1490 Ma	Hbl-Ms	516 ± 52 410 ± 54
Central Kalkadoon Domain	$4.2^{+1.9}_{-2.1}$°C/M	1490–1473 Ma	Ms-Bt	410 ± 54 329 ± 58
(Average cooling rate)	$3.9^{+1.7}_{-1.4}$°C/Ma	1521–1473 Ma	Hbl-Bt	516 ± 52 329 ± 58
Western belt				
Sybella Domain	$1.0^{+0.5}_{-0.3}$°C/Ma	1575–1523 Ma	Metamorphism-Hbl	600 ± 50 532 ± 54
Sybella Domain	$1.4^{+4.0}_{-3.5}$°C/Ma	1523–1505 Ma	Hbl-Hbl	532 ± 54 507 ± 52
Sybella Domain	$0.9^{+0.5}_{-0.5}$°C/Ma	1505–1397 Ma	Hbl-Ms	507 ± 52 406 ± 50
Sybella Domain	$3.6^{+3.3}_{-3.0}$°C/Ma	1397–1376 Ma	Ms-Bt	406 ± 50 331 ± 58
(Average cooling rate)	$1.4^{+0.2}_{-0.3}$°C/Ma	1575–1376 Ma	Metamorphism-Bt	600 ± 50 331 ± 58

5.1.4. Mitakoodi Domain

Sample MMB03 is a foliated metabasalt collected from the Malbon Group. It comprises millimeter-sized amphibole porphyroblasts in a matrix of prismatic euhedral amphibole and elongated aggregates of plagioclase and quartz. Amphibole porphyroblasts are green to blue with subhedral shapes and are partially altered by chlorite. Plagioclase shows concentric zoning but is highly altered by sericite.

Sample CF05 is a muscovite-schist collected from the Malbon Group, 8 km northeast of MMB03. The sample comprises quartz (~30%), biotite (~30%), plagioclase (~25%), muscovite (~10%), and accessory ilmenite (Figure S8d). The dominant foliation is defined by alternating mica-rich layers, marked by preferred orientation of euhedral biotite, muscovite, and felsic-rich domains (quartz + plagioclase).

5.1.5. Doherty Domain

Sample AMS01 is a metadolerite collected from the Soldiers Cap Group in the Doherty Domain, west of the Cloncurry fault. The sample comprises mainly millimeter-sized amphibole (~55% vol.%) and mildly sericitized feldspar (~40%). The foliation is defined by shape preferred orientation of amphibole and plagioclase (Figure S9a). Amphibole crystals are light brown to dark green, subhedral, and have straight contacts with the surrounding plagioclase. A minor second generation of euhedral brown amphibole occurs along the foliation, which replaces the early green amphibole. Plagioclase is partially altered by sericite.

10.1029/2020TC006129

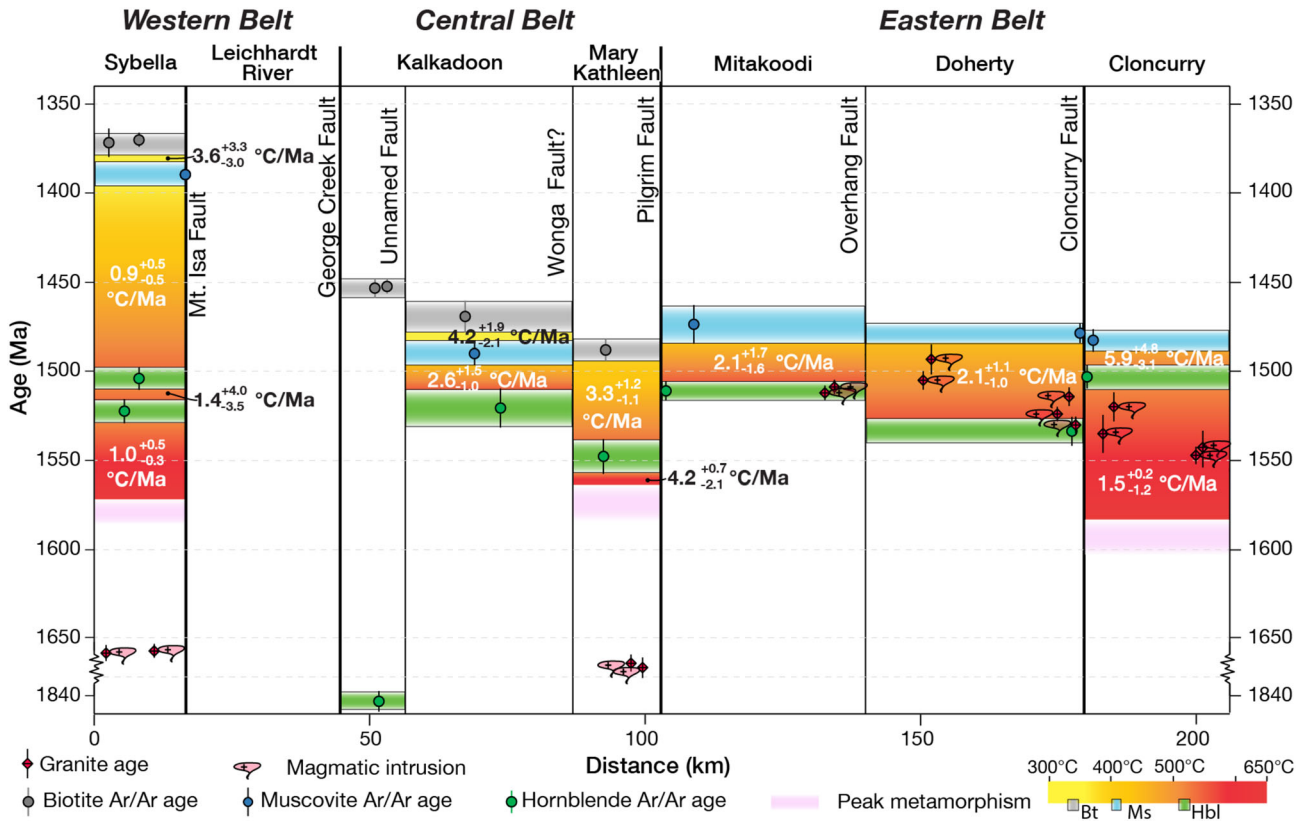

Figure 8. Time versus distance plot of $^{40}Ar/^{39}Ar$ ages along a W-E transect across the Mount Isa Inlier (Line A-A′ in Figure 1). Different domains are subdivided by the major boundary faults. Each of the green, blue, and gray bars represents the cooling age dated from the hornblende, muscovite, and biotite, respectively.

Sample MnMs01 is a biotite-bearing schist collected from the Mount Norna Quartzite, 10 km north of AMS01. The sample is strongly foliated with the pervasive fabric defined by shape preferred orientation of biotite and minor muscovite alternating with quartzo-feldspathic-rich domains (Figure S9b). Quartz has undulose extinction, suggesting intracrystalline deformation. The dominant foliation is interpreted to have formed during the Isan Orogeny, correlative with amphibolite facies metamorphism documented in the Snake Creek anticline (Abu Sharib & Sanislav, 2013; Rubenach & Barker, 1998).

5.1.6. Cloncurry Domain

Sample AML01 is an amphibolite collected from the Snake Creek anticline, east of the Cloncurry fault. The sample is composed of amphibole, plagioclase, minor relicts of clinopyroxene, rare orthopyroxene, and minor interstitial quartz and magnetite. Primary porphyritic amphibole occurs as centimeter-sized grains that have a decomposed core with corrosion relic texture (Figure S9c). Plagioclase occurs as fine millimeter-scale grains with weak oscillatory zoning. Locally, overgrowth of light green amphiboles are millimeter-sized and euhedral, suggesting an overprint origin.

Sample LCF01 is a muscovite schist collected from the Snake Creek anticline, 4 km southwest of AML01. The sample has a pervasive foliation defined by the alignment of euhedral muscovite and minor brown biotite, interlayered with flattened quartz grains (Figure S9d). The orientation of the grains indicates that they are synkinematic to the dominate foliation.

5.2. Cooling Ages

Sixteen analyses, including nine hornblende, four muscovite, and three biotite single-grain aliquots, yielded flat ^{39}Ar release spectra (Figures 5–7). These statistically robust plateaus show low scatter, have p values >0.05, with ~70% or more of ^{39}Ar released over a minimum of three consecutive steps agreeing at 95%

confidence level. These results are combined with the recalculated ages from previous studies to produce the most accurate $^{40}Ar/^{39}Ar$ thermochronological data set available for this region.

5.2.1. Western Belt

In the western belt, hornblende Sample SG01 from the Sybella Granite yielded a plateau age of 1523 ± 7 Ma with 69% of ^{39}Ar released in the last six steps at a mean square weighted deviation (MSWD) value of 2.13 and a p value of 0.06. The K/Ca shows a consistent ratio of 0.210 ± 0.006 over the plateau with little variation on each step, which indicates a homogenous signature of the dated mineral and a volume diffusion behavior during the step heating experiment. Five kilometers northeast of SG01, from the country rock of the Sybella granite, amphibole from Sample CRS01 yielded a plateau age of 1505 ± 6 Ma (81.3% ^{39}Ar released; MSWD = 0.89, $p = 0.52$) over nine steps. The step age remains concordant in the $^{40}Ar/^{39}Ar$ age spectrum except for the last three steps that have relatively large errors, where the K/Ca ratio decreased to below 0.05. A previous study in this domain reported muscovite and biotite cooling ages of circa 1400 and 1370 Ma, respectively (Spikings et al., 2002).

5.2.2. Central Belt

Of the eight samples collected from the central belt of the Mount Isa Inlier, four hornblende, three biotite, and one muscovite analyses gave robust $^{39}Ar/^{40}Ar$ ages. The oldest cooling age was produced from hornblende in a migmatite amphibolite (KLB1604) of the Kalkadoon Domain (ca. 1.85 Ga high-grade metamorphic rock, Page & Williams, 1988), which yielded a plateau age of 1843 ± 6 Ma (74% of ^{39}Ar released at 10 steps; MSWD = 0.72, $p = 0.69$). One kilometer to the west, biotite from a biotite gneiss (KLB1602) gave a plateau age of 1454 ± 5 Ma (91% of ^{39}Ar released at 10 steps; MSWD = 0.90, $p = 0.52$). Further to the northeast, muscovite from the Kalkadoon granite (KG07) yielded a plateau age of 1490 ± 6 Ma (94% of ^{39}Ar released at 14 steps; MSWD = 0.28, $p = 0.99$). Within the same domain, hornblende from metabasalt MLMB01yielded a plateau age of 1521 ± 11 Ma (100% of ^{39}Ar released at eight steps; MSWD = 1.26, $p = 0.36$). Across the Mount Remarkable fault further north, hornblende from the metadolerite MDL01 yielded a similar age of 1527 ± 3 Ma (100% of ^{39}Ar released at 15 steps; MSWD = 0.32, $p = 0.1$). Biotite from the circa 1.86 Ga Kalkadoon granite (KG03), 15 km further north, yielded a plateau age of 1534 ± 5 Ma (90% of ^{39}Ar released at nine steps; MSWD = 1.13, $p = 0.34$). To the east, between the Pilgrim fault and the Kalkadoon-Leichhardt basement (Figure 6), hornblende from meta-gabbro (LCG01) in the Mary Kathleen Domain yielded a mini-plateau age of 1549 ± 10 Ma (66% of ^{39}Ar released at six steps; MSWD = 0.32, $p = 0.90$), while biotite from a nearby Wonga Granite (WG01) produced a plateau age of 1489 ± 6 Ma (98% of ^{39}Ar released at 12 steps; MSWD = 0.54, $p = 0.89$).

5.2.3. Eastern Belt

In the eastern belt, three hornblende and three muscovite aliquots gave six robust $^{39}Ar/^{40}Ar$ ages. In the Mitakoodi Domain on the west, hornblende from a metabasalt (MMB03) gave a plateau age of 1512 ± 5 Ma (84% of ^{39}Ar released at 10 steps; MSWD = 0.49, $p = 0.88$), while muscovite from nearby muscovite schist Sample CF05 yielded a plateau age of 1474 ± 11 Ma (100.0% ^{39}Ar released at 4 steps; MSWD = 1.82, $p = 0.14$). Further east in the Doherty Domain, between the Cloncurry and Overhang faults (Figure 7), a hornblende age of 1534 ± 8 Ma (93% ^{39}Ar released at 8 steps; MSWD = 0.84, $p = 0.55$) was obtained for amphibolite Sample AMS01 and a muscovite age of 1479 ± 5 Ma (99% ^{39}Ar released at 16 steps; MSWD = 1.1, $p = 0.35$) for muscovite schist Sample MnMs01. For comparison, hornblende from amphibolite (AML01) in the Cloncurry Domain, east of the Cloncurry fault (Figure 7), produced a plateau age of 1504 ± 7 Ma (100% of ^{39}Ar released at 18 steps; MSWD = 1.02, $p = 0.42$), while muscovite from a nearby muscovite schist sample (LCF01) yielded an Argon plateau age of 1483 ± 6 Ma (100% of ^{39}Ar released at 14 steps; MSWD = 0.5, $p = 0.93$).

Sixteen analyses from this study yield plateau ages with ~70% or greater ^{39}Ar released. The range of step-heating ages is considered to reflect cooling ages rather than distinct mineral growth/recrystallization events based on the following observations. (1) The microstructures of the samples, all from high-grade amphibolite facies areas, suggest that the dated mica is stable and did not break down to other mineral phases during the peak metamorphism. High peak-metamorphism temperatures and partial melting likely led to relatively dry post-thermal-peak conditions, inhibiting late mica recrystallization. (2) The metamorphic pressure-temperature (P-T) paths of the sampling areas (see section 6.1 and Figure 9) show no reheating or thermal disturbance. (3) The normal isochron spectra show a similar portion of $^{40}Ar/^{36}Ar$

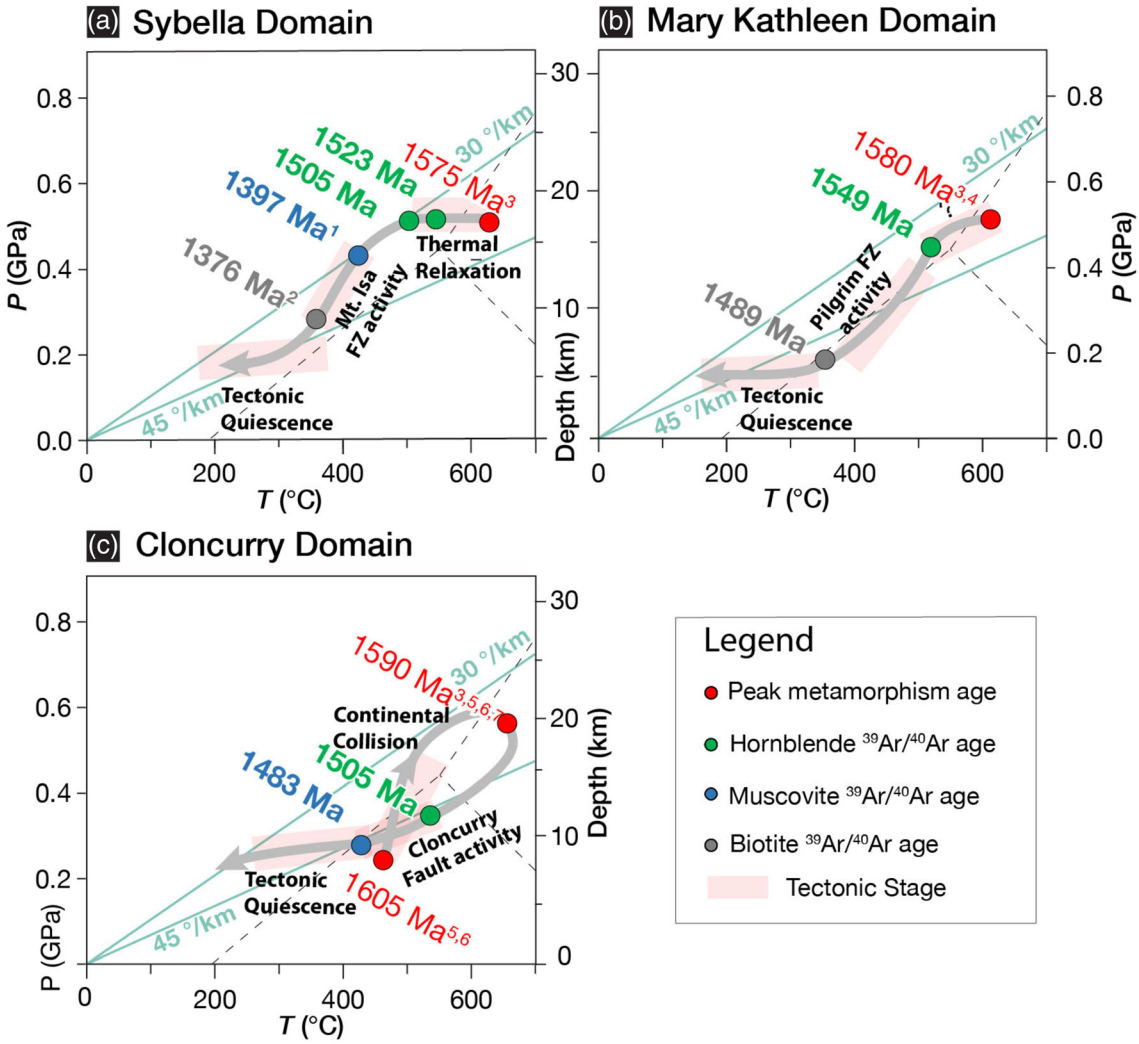

Figure 9. Reconstructed P-T evolution and tectonic interpretation of the Sybella (Figure 9a, following Blenkinsop, 2005; Rubenach, 1992), Mary Kathleen (Figure 9b, following Hand & Rubatto, 2002; Reinhardt, 1992a, 1992b), and Cloncurry domains (Figure 9c, following Foster & Rubenach, 2006; Pourteau et al., 2018; Rubenach et al., 2008; Sayab, 2006). Dashed lines represent the limits of stability of the aluminosilicate polygraphs silicates. The green lines represent the 30°C/km geothermal gradient extends 25 km through the crust and are used as a guide to constrain thermal relaxation during periods of tectonic quiescence, that is, stages of long-term continental erosion. Peak metamorphism ages and $^{39}Ar/^{40}Ar$ age are referred from previous works: 1 = Perkins et al. (1999), 2 = Spikings et al. (2002), 3 = Hand and Rubatto (2002), 4 = Foster (2003), 5 = Rubenach et al. (2008), 6 = Pourteau et al. (2018), and 7 = Giles and Nutman (2002).

versus $^{39}Ar/^{36}Ar$ and a corresponding steady minimum plateau age at each step heating, which suggests consistent diffusion in a closure system with little external impact. Based on these lines of evidence, the obtained $^{40}Ar/^{39}Ar$ ages are interpreted to have recorded post-thermal-peak cooling through the minerals' closure temperatures, rather than ages of late recrystallization (or neocrystallization), reheating or hydrothermal episodes.

5.3. Cooling Rate Estimation

To monitor the cooling behavior within and between different tectonic domains, cooling rates calculations were conducted using specific closure temperatures from different mineral pairs (Figure 8). The cooling rate values are reported as the median value and 90% interpercentile range between 5% and 95% ($\frac{I_3}{I_1}$) to minimized the mathematical errors associated with Monte Carlo simulations (detailed explanations are given in Text S2 of the supporting information). In the western belt, the Sybella Domain recorded an initial cooling

10.1029/2020TC006129

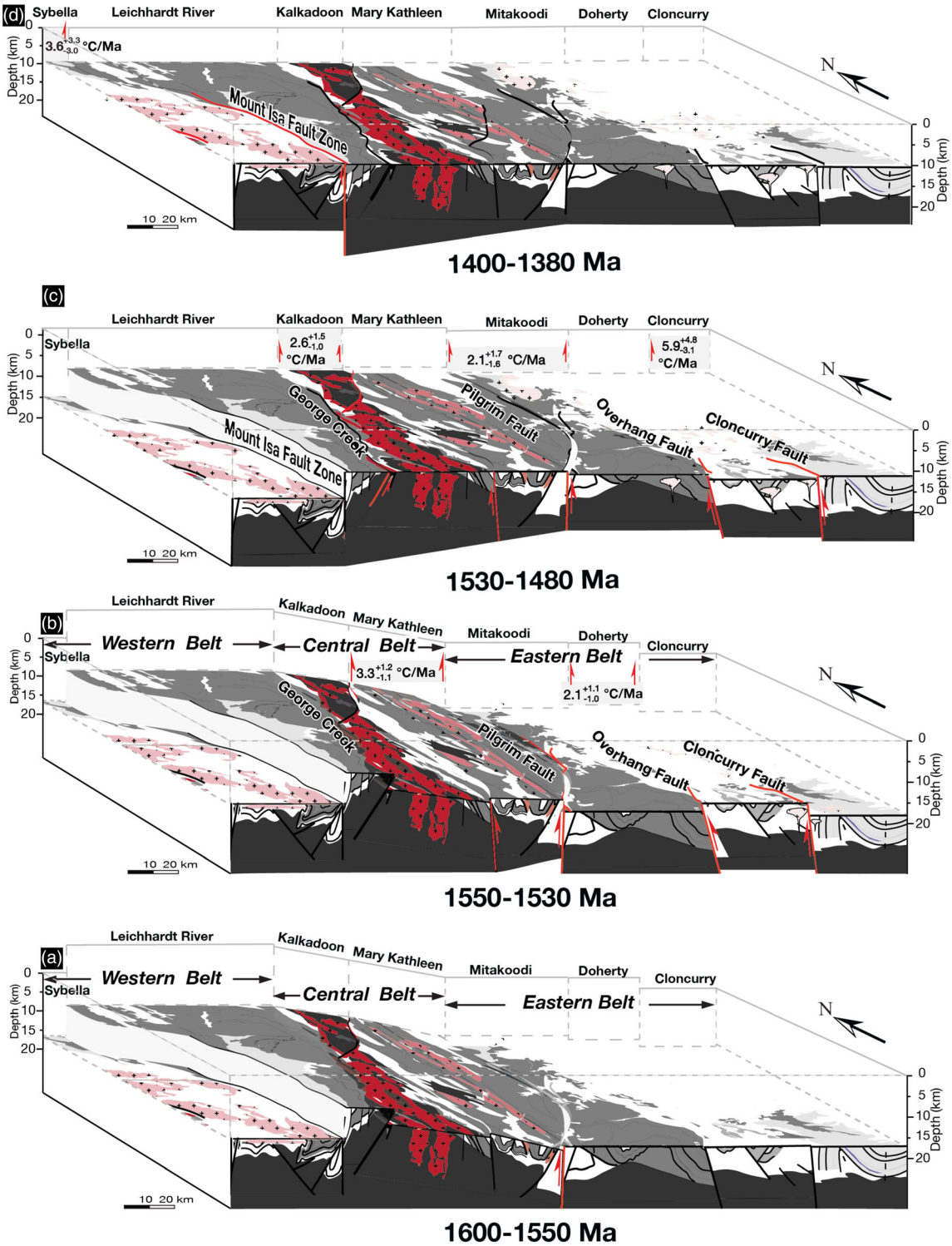

Figure 10. (a–c) Interpretation of the exhumation history in the Mount Isa Inlier from 1600 to 1380 Ma. (a) At 1600–1580 Ma, presently exposed domains were at different crustal levels, as indicated by different peak pressure conditions during the Isan Orogeny. (b) At 1550–1520 Ma, postorogenic extension was accommodated along preexisting, generally steep faults. The Pilgrim fault acted as an east dipping normal fault, accommodating differential vertical motion between the central and eastern belts. In the eastern belt, the Doherty Domain was exhumed at circa 1.53 Ga due to the activation of the east dipping Cloncurry fault (Blenkinsop et al., 2008) and possibly also the Overhang fault. (c) At 1530–1480 Ma, extensional faulting continued. In the eastern belt, the Mitakoodi and Cloncurry domains were exhumed. In the central belt, the eastern Kalkadoon Domain was exhumed either through block tilting to the west, or differential uplift relative to the western Kalkadoon and Mary Kathleen domains. (d) At 1400–1380 Ma, following a period of tectonic quiescence, the Mount Isa fault was finally reactivated, whereas the remainder of the inlier remained a coherent crustal block.

from 532 ± 54°C (Hbl) to 507 ± 52°C (Hbl) during 1.52–1.50 Ga at $1.4^{+4.0}_{-3.5}$°C/Ma, followed by a slower cooling from 507 ± 52°C (Hbl) to 406 ± 50°C (Ms) between 1.50 and 1.40 Ga at $0.9^{+0.5}_{-0.5}$°C/Ma and lastly cooling from 406 ± 50°C (Ms) to 331 ± 58°C (Ms) during 1.40–1.37 Ga at $3.6^{+3.3}_{-3.0}$°C/Ma (Table 1). In the central belt, west of the Pilgrim fault, the Mary Kathleen Domain recorded cooling from 524 ± 48°C (Hbl) to 328 ± 58°C (Bt) between 1.55 and 1.49 Ga at $3.3^{+1.2}_{-1.1}$ °C/Ma, while the Kalkadoon Domain further west cooled from 516 ± 52°C (Hbl) to 410 ± 54°C (Ms) during 1.52–1.49 Ga at $2.6^{+1.5}_{-1.0}$ °C/Ma, and 410 ± 54°C (Ms) to 329 ± 58°C (Bt) between 1.49 and 1.47 Ga at $4.2^{+1.9}_{-2.1}$°C/Ma. In the eastern belt, the Mitakoodi Domain, in the west, recorded cooling from 486 ± 54°C (Hbl) to 408 ± 50°C (Ms) between 1.51 and 1.47 Ga at $2.1^{+1.7}_{-1.6}$° C/Ma. The Doherty Domain, between the Cloncurry and Overhang faults, recorded a cooling rate of $2.1^{+1.1}_{-1.0}$ °C/Ma from 526 ± 48°C (Hbl) to 409 ± 50°C (Ms) during 1.53–1.48 Ga. To the east of the Cloncurry fault, the Cloncurry Domain appears to have cooled from 517 ± 52°C (Hbl) to 397 ± 49°C (Ms) between 1.50 Ga and 1.48 Ga at a rate of $5.9^{+4.8}_{-3.1}$°C/Ma (Table 1).

6. Discussion

6.1. Diachronous Cooling and Exhumation of the Crustal Domains

To further evaluate the main controlling factors on the cooling ages from the different tectonic domains, the $^{40}Ar/^{39}Ar$ geochronological results are combined with published geochronological and petrological constraints (Blenkinsop, 2005; Foster & Rubenach, 2006; Pourteau et al., 2018; Rubenach, 1992; Rubenach et al., 2008; Sayab, 2006) to reconstruct retrograde P-T paths (Figure 9) and decipher the timing of the various fault zones and the exhumation histories of the crustal domains (Figures 8 and 10).

6.1.1. Western Belt

The Sybella Domain recorded prograde metamorphism at circa 1575 Ma, marked by the successive growth of cordierite and andalusite or sillimanite, suggesting heating from 520–550°C at 0.3–0.4 GPa to ~560–650°C at 0.4–0.6 GPa (Blenkinsop, 2005). Retrograde kyanite (Rubenach, 1992) indicates near isobaric cooling through hornblende closure temperatures of 532 ± 54°C at 1523 ± 7 Ma and of 507 ± 53°C at 1505 ± 6 Ma (Figure 9a). This initial cooling was coeval with most of the other domains in the inlier. However, biotite cooled below ~330°C > 130 Myr later at circa 1375 Ma (Spikings et al., 2002). Given that muscovite near the Mount Isa fault was dated at circa 1400 Ma, only ~20 Myr before biotite cooled, we suggest that the Sybella Domain cooling below ~330°C was associated with the activation of the Mount Isa fault. With muscovite closure temperature of 405 ± 50°C recalculated from the published result (Spikings et al., 2002), the Mount Isa fault zone likely had accommodated significant exhumation of the Sybella Domain, possibly from ~14 km to ~9 km (Figures 10c and 10d) at a rate of ~0.25 mm yr^{-1} and with a maximum cooling rate of $3.6^{+3.3}_{-3.0}$°C/Ma.

6.1.2. Central Belt

In the western Kalkadoon Domain of the central belt (Figure 6), the circa 1.87–1.84 Ga amphibolite-facies basement (Bierlein et al., 2008; Page & Williams, 1988) preserves a post-Barramundi Orogeny cooling age of circa 1.84 Ga through 520 ± 50°C. The cooling of the high-grade basement shortly after the Barramundi Orogeny is consistent with normal faulting activity of the George Creek fault (which bounds the basement horst to the east; Figure 1) during deposition of the Leichhardt Superbasin (Jackson & Southgate, 2000). We, therefore, infer that the cooling of the western Kalkadoon Domain through ~520°C was associated with the exhumation of the basement in a Leichhardt-aged horst. On the other hand, the eastern Kalkadoon Domain cooled through 520 ± 50°C at circa 1.52 Ga (Figure 8). The contrasting thermal records from the two segments of the Kalkadoon Domain suggest that either the eastern segment was buried during the Isan Orogeny (with the domain tilting to the east possibly caused by west verging thrusts and/or the loading of foreland basin deposits) and was subsequently exhumed at circa 1.52 Ga, or there was a crustal-scale boundary fault between the western and eastern Kalkadoon Domain.

Further to the northeast, biotite from north of the Mount Remarkable fault cooled below ~330°C at circa 1535 Ma, 15 Ma earlier than the hornblende cooling below ~550°C to the south of the fault. The thermal discontinuity separated by the Mount Remarkable fault is consistent with the metamorphic isograd jump across this fault (Figure 4; Foster & Rubenach, 2006), suggesting that the Mount Remarkable fault is a crustal boundary between the northern and southern sections of the central belt.

The Mary Kathleen Domain records the shortest duration (10–30 Myr) from metamorphic peak temperature (~600°C) at circa 1575 Ma (Hand & Rubatto, 2002; Reinhardt, 1992a, 1992b) to cooling through 524 ± 48°C at 1549 ± 10 Ma (Figure 9b). The kyanite growth after sillimanite reported from schist in the Mary Kathleen Domain (Reinhardt, 1992a) suggests that cooling below ~550°C (i.e., the temperature of the aluminum silicate triple point) took place near peak pressure (~0.5 GPa; Reinhardt, 1992a). This well-constrained anticlockwise P-T-t path represents an episode of relatively rapid decompression and exhumation immediately following peak metamorphism (Figures 8 and 9b). We interpret this significant early (ca. 1.57 Ga to ca. 1.55 Ga) decompression and cooling below the Ar closure temperature of biotite (~330°C) to reflect the activation of the subvertical but slightly east dipping Pilgrim fault as a normal fault which exhumed the amphibolite facies Mary Kathleen Domain (Figure 10). The relative sense of vertical motion along this fault may have reversed afterward, leading to the cooling of the Mitakoodi Domain to its east through the hornblende closure temperature (~520°C) at circa 1.51 Ga (Figures 8, 10b, and 10c).

In the central belt, biotite $^{40}Ar/^{39}Ar$ ages become progressively younger westward (Figure 8). Because no systematic difference in closure temperature could be resolved (Table S3), we infer that cooling of the central belt was diachronous: from 1550 to 1520 Ma for hornblende (~520°C) and 1490 to 1460 Ma for biotite (~350°C). The lack of post-1600 Ma magmatic record in the central and western belts precludes magmatic cooling as a mechanism for cooling in the central belt. Therefore, we attribute the diachronous cooling to differential tectonic exhumation within the central belt, either by E-W block tilting, or by east to west diachronous uplifting of hosts with the Mary Kathleen Domain the earliest, and the western Kalkadoon Domain the latest (Figures 8, 10b, and 10c).

6.1.3. Eastern Belt

The metamorphic history in the Cloncurry Domain near the sample locality recorded heating from 450–520°C at 0.3–0.45 GPa (1605 Ma) to 520–630°C at 0.45–0.6 GPa (1590 Ma, Figure 10c) (Foster & Rubenach, 2006; Giles & Nutman, 2002; Pourteau et al., 2018; Rubenach et al., 2008; Sayab, 2006). The successive overgrowths of cordierite and andalusite by kyanite and, later, by sillimanite before their being replaced by andalusite indicate a clockwise P-T path culminating at moderate pressures (Abu Sharib & Sanislav, 2013; Foster & Rubenach, 2006; Rubenach et al., 2008; Rubenach & Lewthwaite, 2002). Our $^{40}Ar/^{39}Ar$ results indicate that the Cloncurry Domain cooled to 517 ± 53°C at 1504 ± 7 Ma, that is, ≥70 Myr after the peak metamorphism at a cooling rate of approximately 1.2°C/Ma, and through 397 ± 49°C at 1483 ± 6 Ma, with an accelerated cooling rate of $5.9^{+4.8}_{-3.1}$°C/Ma.

All domains of the eastern belt cooled synchronously through ~400°C at circa 1480 Ma, although their cooling through ~520°C occurred diachronously between 1535 and 1505 Ma (Figure 8). For example, the cooling in the Cloncurry Domain occurred at circa 1505 Ma, 20–30 Myr later than the adjacent Doherty Domain. Further west, the Mitakoodi Domain shows an intermediate cooling age at 1512 ± 5 Ma. The heterogeneous cooling age between different geological domains cannot be explained by systematic differences in mineral closure temperature (Table S3). We thus evaluate two alternative driving mechanisms for the cooling of the eastern belt: postmagmatic thermal relaxation, and tectonic exhumation.

Mechanism 1: Cooling ages in the eastern belt represent resetting of the argon systematics associated with local granitic intrusions. Granitic intrusions in the eastern belt near the sample localities are dated at circa 1.53 to 1.51 Ga (Page & Sun, 1998; Pollard & McNaughton, 1997), comparable to the range of the hornblende $^{40}Ar/^{39}Ar$ cooling ages of between circa 1.53 and 1.50 Ga. The best example for argon systematics resetting is preserved in the Doherty Domain, where the hornblende dated from an amphibolite adjacent to Mount Angelay granite gave an $^{40}Ar/^{39}Ar$ cooling age within error of the granite (1534 ± 8 Ma vs. 1529 ± 4 Ma; Pollard & McNaughton, 1997). Nevertheless, it is unlikely that cooling ages in the Cloncurry Domain were all related to granite emplacement. For example, hornblende from an amphibolite near the circa 1.53 Ga Saxby granite yielded a circa 1.50 Ga $^{40}Ar/^{39}Ar$ cooling age, which is too young to be related to the magmatic cooling. In the Mitakoodi Domain, the dated hornblende from the Mitakoodi metabasalts is too distant (45 km) from the nearest circa 1.51 Ga Wimberu granite to acquire an argon resetting age. Thus, magmatism alone cannot account for the cooling history of this domain.

Mechanism 2: Initial cooling (through ~520°C) within the eastern belt was controlled by normal faulting. In this case, the Doherty Domain, which records the oldest cooling age in the eastern belt, exhumed earliest at circa 1.53 Ga due to normal faulting of the east dipping Cloncurry fault (Blenkinsop et al., 2008). This was followed by the exhumation of the Mitakoodi and Cloncurry domains at circa 1.51–1.50 Ga (Figures 10b and 10c). This interpretation involves repeated activation of the domain-bounding faults with varying fault kinematics. After circa 1.50 Ga, the eastern belt appears to have behaved as a coherent crustal block, all recording statistically indistinguishable circa 1480 Ma muscovite $^{40}Ar/^{39}Ar$ ages (Figures 8 and 10).

In summary, the postorogenic evolution of the Mount Isa Inlier was characterized by heterogeneous but consistently slow cooling and exhumation, driven mostly by diachronous fault movements. Reconstructed fault movements indicate that both pre-Isan basin-controlling normal faults (e.g., the Pilgrim and Cloncurry faults; Blenkinsop et al., 2008) and Isan aged reverse faults (e.g., the Overhang fault; Baker et al., 2001) were reactivated as postorogenic normal faults during a post-Isan extensional phase.

6.2. Final Assembly of Nuna by "Soft" Collision

The uncommon association of crustal shortening with low-P/T metamorphism and counterclockwise P-T evolutions observed during the Isan Orogeny, as well as in other Mesoproterozoic orogenic belts (i.e., the Halls Creek orogen) in Australia, have been noticed and debated for over four decades (Bell, 1983; Bell et al., 1992; Betts et al., 2006, 2007; Etheridge et al., 1987; Foster & Rubenach, 2006; Loosveld, 1989; Rubenach, 1992; O'Dea, Lister, Betts, & Pound, 1997). Here, we complement and add to the previous studies and discuss the tectonic regime of the unusual Isan Orogeny by incorporating our reconstruction of the regional postorogenic cooling and exhumation history.

According to a worldwide database of mountain ranges actively undergoing denudation/exhumation, surface erosion shares a linear relationship with topographic relief (Pinet & Souriau, 1988). In the Mount Isa Inlier, the exhumation following the Isan Orogeny was likely facilitated by a combination of postorogenic normal faulting and surface erosion. The average postpeak metamorphic exhumation rates estimated for the individual crustal domains of the Mount Isa Inlier (between 1°C/Ma and 6°C/Ma) suggest an overall erosion rate of less than <0.5 mm yr^{-1}. By taking a uniformitarian approach and applying the updated relationship between erosion rate and regional-scale relief of Montgomery and Brandon (2002), the slow exhumation rates suggest that, following the Isan Orogeny, the Mount Isa Inlier had a local relief of less than 1,000 m above sea level. This is consistent with previous studies which suggested that the Isan Orogeny was associated with low-elevation mountain ranges (McLaren et al., 2005) and had limited tectonic burial (reflected by low peak pressure conditions; Figure 9) and scarce postorogenic molasse-type flexural sedimentary basins (McConachie et al., 1993; Southgate et al., 2000). The shallowness of crustal imbrication (Abu Sharib & Sanislav, 2013; Bell, 1991; MacCready, 2006) and width of the resulting orogenic belt formed during the juxtaposition of Australia against Laurentia at circa 1.60 Ga were previously proposed to have resulted in a "soft collision" (Nordsvan, Collins, & Li, 2018) of possibly thin and hot continental regions (McLaren et al., 2005; Pourteau et al., 2018).

6.3. Postorogenic Exhumation: Insight Into the Orogen's Thermal Regime

Mechanisms that drive orogenic exhumation vary from orogen to orogen due to their distinct tectonic and thermal regimes. To determine the exhumation mechanism of Proterozoic orogens, it may benefit from a comparison with well-studied modern analogs. Modern orogens can be subdivided into three categories: "small cold orogens" (SCOs), "transitional orogens" (TOs), and "large hot orogens" (LHOs) based on their thermal regimes and magnitude (Beaumont et al., 2006; Jamieson et al., 2002). Although no quantitative criteria (e.g., specific sizes or temperature values) have been provided to classify the orogeny types, orogens such as the Cascadia, Pyrenees, and Abitibi are regarded as SCOs, whereas Tibet, Grenvillian, Variscan, Andes, and Trans Hudson are considered as LHOs (Beaumont et al., 2006). While SCOs are characterized by rigid crust deformation with little ductile deformation, LHOs (such as the Himalayan) typically undergo prolonged crustal heating and develop a central elevated plateau above a weak lower crust (Jamieson & Beaumont, 2013). Synorogenic to postorogenic collapse is thought to be common for LHOs, which is driven by the isostatic instability of hot, thickened, melt-weakened lower crust underneath the plateau (Jamieson & Beaumont, 2013). For example, LHOs like the Variscan, Svecofennian, and Grenvillian orogens all contain

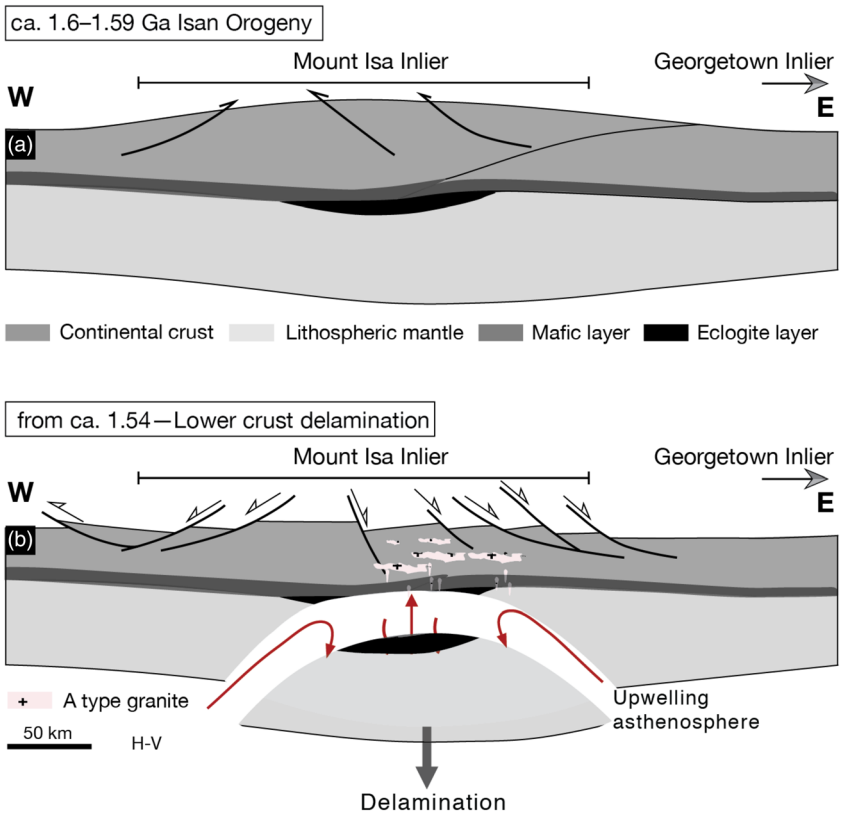

Figure 11. Conceptional model for the tectonic evolution of the Mount Isa Inlier from 1600 to 1540 Ma. (a) The circa 1600 Ma continental collision event in the Mount Isa Inlier recorded westward accretion of the Georgetown Inlier with local crustal thickening within the eastern belt. (b) The locally thickened crust was delaminated and replaced by the upwelling asthenosphere. Elevated geotherm by hot mantle upwelling, together with water released from the sinking lower crust and reduced pressure caused by orogenic collapse, induced widespread postkinematic felsic to mafic magmatism.

metamorphic core complexes or "core complex-like systems" involving domal uplift or vertical extrusion of middle to lower crustal rocks (Korja et al., 2009; Rubio Pascual et al., 2013; Rivers, 2012; Schulmann et al., 2008), whereas SCOs are comparatively cold and rheologically stronger and tend not to result in orogenic collapse but with erosion being the dominant mechanism for exhumation (Jamieson & Beaumont, 2013). The Mount Isa Orogen, which had a high thermal regime (McLaren et al., 2005) and large lateral extent (over 120,000 km^2), is more comparable with LHO-type orogens.

6.4. Exhumation History and Driving Mechanism for the Mount Isa Inlier

In the Mount Isa Inlier, the circa 1530–1480 Ma interval was marked by cooling and exhumation throughout the entire inlier. This was broadly coeval with voluminous circa 1550–1490 Ma magmatism in the eastern belt. The chemical composition and temporal evolution of this magmatic phase may, therefore, provide constraints on the tectonic mechanisms that controlled exhumation. Late orogenic to postorogenic intrusions in the eastern belt consist of localized circa 1550 Ma trondhjemite (Mark, 2001) west of the Cloncurry fault (Figure 7) and widespread voluminous circa 1540–1490 Ma A-type granitoids. The trondhjemite, which is typically foliated, is characterized by high Al_2O_3 contents, low heavy rare earth element content, and no Sr anomaly, suggesting that it was derived by partial melting of a hydrated mafic source possibly at >0.8–1.0 GPa (Mark, 2001). The A-type intrusive rocks range from monzodiorite and monzogranite to syenogranite and exhibit Sr and Eu negative anomalies with elevated high field strength element contents (Blenkinsop, 2005; Mark, 2001). They were likely produced at >900°C and <0.8–1.0 GPa from a tonalitic to granodioritic source (Mark, 2001). The εNd values of approximately −3.5 to −2.5 of the A-type rocks indicate that they were likely derived from the Palaeoproterozoic basement rocks (Mark, 2001; Page & Sun, 1998).

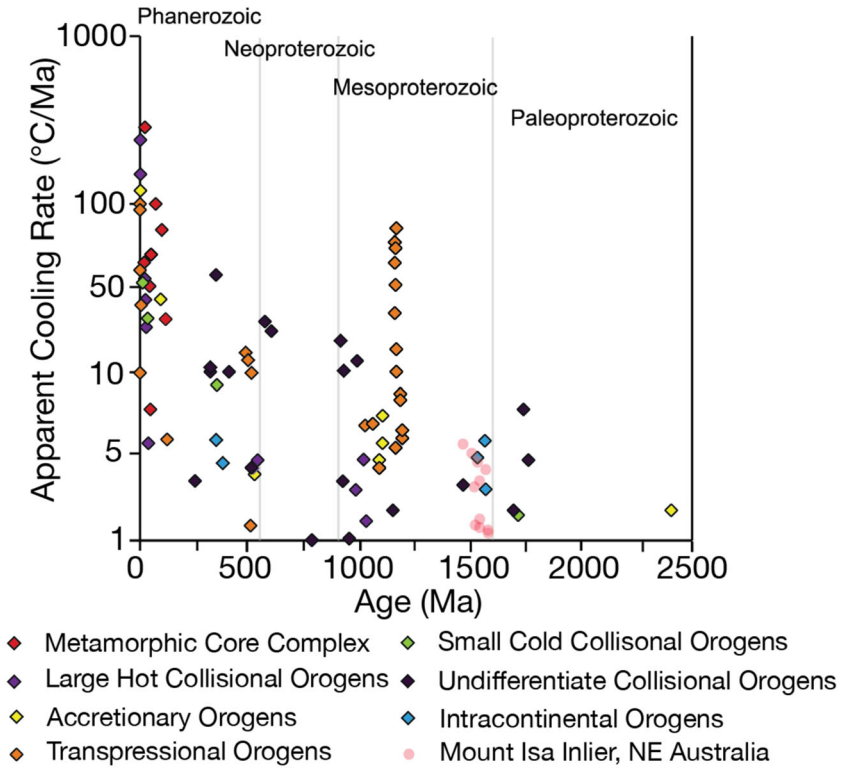

Figure 12. Plot of global orogenic cooling rates (modified after Scibiorski et al., 2015). Orogens are categorized by tectonic settings with the cooling rates of previous studies source from Scibiorski et al. (2015) and references therein. New data from the Mount Isa Inlier are shown in pink diamonds.

Previous studies (Betts et al., 2009) suggest that these A-type granitic rocks were associated with a hotspot track extending from the South Australian Craton (ca. 1.59 Ga) to the Mount Isa Inlier (50 Myr later). However, this mantle plume interpretation would predict juvenile magma generation by mantle decompression melting (White, 2013), which has not been reported from this region (e.g., Mark, 2001).

By integrating the magmatic evolution with regional terrane exhumation history, we propose the alternative scenario where orogenic collapse triggered regional metamorphism and magmatism. The geochemical evolution of magmatism from circa 1550 to 1490 Ma indicates heating in the lower crust of the eastern Mount Isa Inlier was broadly contemporaneous with the early exhumation and cooling of the middle crust, as constrained by the $^{39}Ar/^{40}Ar$ ages. We note that the circa 1550–1490 Ma intrusions are restricted to the eastern belt that recorded crustal thickening during the circa 1600 Ma orogeny (Pourteau et al., 2018) (Figure 11a). Therefore, we propose that, as suggested for other orogens (e.g., Bird, 1979; England & Houseman, 1989; Jiménez-Munt et al., 2008; Li et al., 2010; Meng et al., 2012; Yao et al., 2012), lower crustal heating in the Mount Isa Inlier was caused by the delamination of a predominantly mafic lower crust, possibly due to eclogitization. Delamination of the dense orogenic root would be accompanied by crustal isostatic rebound and extension (orogenic collapse; Li et al., 2010). Water released from the eclogitized mafic lower crust might have triggered the generation of the 1550 Ma trondhjemite at moderate temperatures (~800°C; Mark, 2001) and driven a pressure decrease due to orogenic collapse (Li et al., 2010), whereas the subsequent local influx of hot asthenospheric mantle would have resulted in high-temperature magmatism (>900°C) during 1540–1490 Ma (Figure 11b).

6.5. Slow Cooling Proterozoic Orogens

To compare the cooling behavior of the Mount Isan orogen with global orogens, the cooling rates reported in this study are plotted with data from global orogens younger than 2.5 Ga (Figure 12). The figure shows that cooling rate decreases with increasing orogen ages (Dunlap, 2000). Phanerozoic orogens commonly experienced medium to fast cooling (>50°C/Ma). Precambrian orogens rarely cooled faster than 10°C/Ma, except

for the Albany-Fraser orogen where fast exhumation was controlled by transpressional faulting (Scibiorski et al., 2015). The Mount Isa Inlier, similar to other Precambrian orogens, also shows a slow cooling signature. Several factors have been proposed to explain the slow cooling of Precambrian orogens, including (1) radiogenic heating by radioactive elements from intrusions (McLaren et al., 1999), (2) the data mainly reflect slow erosion rates during the tectonic quiescence stages (Scibiorski et al., 2015), and (3) partial resetting of the argon cooling age after long-term isothermal residence below the nominal closure temperature (Dunlap, 2000; Warren et al., 2012). To determine which factor(s) provide the dominant control on the slow cooling of Precambrian orogens, further investigations are needed. In the Mount Isa Inlier, radiogenic heating by radioactive elements from the granite has been reported to have generated steep upper crustal thermal gradients prior to the Isan Orogeny. Thus, we propose that the slow cooling during the Isan Orogeny may have been caused by the combination of low-elevation (thus slow erosion) due to a soft collision and possibly radiogenic heating by existing granites in the crust (McLaren et al., 2005).

7. Conclusions

New high-precision $^{39}Ar/^{40}Ar$ thermochronology data reveal a diachronous but consistently slow (generally <5°C/Ma) cooling of the Mount Isa Inlier following the circa 1.60 Ga Isan Orogeny. Contrasting cooling histories across postmetamorphic fault zones are best explained by extensional reactivation of inherited basinal faults and orogenic reverse faults during the orogenic collapse stage. Domain-bounding faults in the central and eastern belts reactivated post 1.60 Ga but before circa 1.48 Ga often with varying fault kinematics through time, leading to diachronous relative uplifting and erosion of different crustal domains. The western belt experienced a slower exhumation compared to the central and eastern belts, but the event lasted until circa 1.38 Ga, controlled by the reactivation of the Mount Isa fault.

The documented prolonged and slow exhumation history suggests that the Isan Orogen was associated with a moderately thickened crust with relatively low relief (likely <1,000 m according to modern analogs). The postorogenic exhumation of the Mount Isa Inlier, together with limited tectonic burial, the relative paucity of regional-scale synorogenic sedimentary basins, and the breadth of orogenic deformation, point to a "soft collision" of a previously thinned (and hot) east Australian continental margin with west Laurentia during the final assembly of the supercontinent Nuna. Such an orogen is atypical of modern collisional orogens but is consistent with Precambrian orogens with higher geothermal gradients. The occurrence of trondhjemite (ca. 1550 Ma) to A-type magmatism (1540–1490 Ma) in the eastern belt during this exhumation process, together with our geochronological constraints on the diachronous normal faulting in the inlier, led us to propose that following the circa 1600 Ma peak Isan Orogeny, part of the mafic lower crust was delaminated due to eclogitization and was replaced by hot mantle materials, resulting in the collapse and exhumation of the orogen.

Acknowledgments

This study was supported by a China Scholarship Council and a Curtin Research Scholarship to J. Y. L. and an Australian Research Council Laureate Fellow grant (FL150100133) to Z. X. L. We thank Caroline Perkins for providing argon released data for recalibrating of $^{40}Ar/^{39}Ar$ ages, I. W. Withnall and G. M. Gibson for introducing the Mount Isa Inlier field geology and fruitful discussions, Sigma Zone company for providing student license for Quantum XL program to make Monte Carlo simulation possible, Hugo Olierook and Celia Mayers for their assistance during the $^{40}Ar/^{39}Ar$ data producing, and Josh Beardmore for helping proof reading the manuscript. We are grateful to Sandra McLaren, three anonymous reviewers, and editor Margaret E. Rusmore for their supportive feedback on the manuscript.

Data Availability Statement

Data sets for this research are available at http://doi.org/10.4121/uuid:bfd7c070-ca86-4f3f-82dd-5bfedf7f0d1b and included in these references: Page and Sun (1998), Perkins and Wyborn (1998), Perkins et al. (1999), and Spikings et al. (2001, 2002).

References

Abu Sharib, A. S. A. A., & Sanislav, I. V. (2013). Polymetamorphism accompanied switching in horizontal shortening during Isan Orogeny: Example from the Eastern Fold Belt, Mount Isa Inlier, Australia. *Tectonophysics*, *587*, 146–167. http://doi.org/10.1016/j.tecto.2012.06.051

Baker, T., Perkins, C., Blake, K. L., & Williams, P. J. (2001). Radiogenic and stable isotope constraints on the genesis of the Eloise Cu-Au deposits, Cloncurry district, Northwest Queensland. *Economic Geology*, *96*(4), 723–742. http://doi.org/10.2113/gsecongeo.96.4.723

Beardsmore, T., Newbery, S., & Laing, W. (1988). The Maronan Supergroup: An inferred early volcanosedimentary rift sequence in the Mount Isa Inlier, and its implications for ensialic rifting in the Middle Proterozoic of northwest Queensland. *Precambrian Research*, *40*, 487–507.

Beaumont, C., Nguyen, M. H., Jamieson, R. A., & Ellis, S. (2006). Crustal flow modes in large hot orogens. *Geological Society, London, Special Publications*, *268*(1), 91–145. https://doi.org/10.1144/gsl.sp.2006.268.01.05

Bell, T., Reinhardt, J., & Hammond, R. (1992). Multiple foliation development during thrusting and synchronous formation of vertical shear zones. *Journal of Structural Geology*, *14*(7), 791–805. https://doi.org/10.1016/0191-8141(92)90041-T

Bell, T. H. (1983). Thrusting and duplex formation at Mount Isa, Queensland, Australia. *Nature*, *304*(5926), 493–497. http://doi.org/10.1038/304493a0

Bell, T. H. (1991). The role of thrusting in the structural development of the Mount Isa Mine and its relevance to exploration in the surrounding region. *Economic Geology*, *86*(8), 1602–1625. http://doi.org/10.2113/gsecongeo.86.8.1602
Bell, T. H., & Rubenach, M. J. (1983). Sequential porphyroblast growth and crenulation cleavage development during progressive deformation. *Tectonophysics*, *92*(1–3), 171–194. https://doi.org/10.1016/0040-1951(83)90089-6
Betts, P. G. (1999). Palaeoproterozoic mid-basin inversion in the northern Mt Isa terrane, Queensland. *Australian Journal of Earth Sciences*, *46*(5), 735–748. http://doi.org/10.1046/j.1440-0952.1999.00741.x
Betts, P. G., Ailleres, L., Giles, D., & Hough, M. (2000). Deformation history of the Hampden Synform in the eastern fold belt of the Mt Isa terrane. *Australian Journal of Earth Sciences*, *47*(6), 1113–1125. http://doi.org/10.1046/j.1440-0952.2000.00839.x
Betts, P. G., Armit, R. J., Stewart, J., Aitken, A. R. A., Ailleres, L., Donchak, P., et al. (2016). Australia and Nuna. *Geological Society, London, Special Publications*, *424*(1), 47–81. http://doi.org/10.1144/sp424.2
Betts, P. G., Giles, D., Foden, J., Schaefer, B. F., Mark, G., Pankhurst, M. J., et al. (2009). Mesoproterozoic plume-modified orogenesis in eastern Precambrian Australia. *Tectonics*, *28*, TC3006. https://doi.org/10.1029/2008TC002325
Betts, P. G., Giles, D., Mark, G., Lister, G. S., Goleby, B. R., & Ailleres, L. (2006). Synthesis of the proterozoic evolution of the Mt Isa Inlier. *Australian Journal of Earth Sciences*, *53*(1), 187–211. http://doi.org/10.1080/08120090500434625
Betts, P. G., Giles, D., & Schaefer, B. F. (2008). Comparing 1800–1600 Ma accretionary and basin processes in Australia and Laurentia: Possible geographic connections in Columbia. *Precambrian Research*, *166*(1–4), 81–92. http://doi.org/10.1016/j.precamres.2007.03.007
Betts, P. G., Giles, D., Schaefer, B. F., & Mark, G. (2007). 1600–1500 Ma hotspot track in eastern Australia: Implications for Mesoproterozoic continental reconstructions. *Terra Nova*, *19*(6), 496–501. http://doi.org/10.1111/j.1365-3121.2007.00778.x
Betts, P. G., & Lister, G. S. (2001). Comparison of the 'strike-slipe' versus 'episodic rift-sag' models for the origin of the Isa superbasin. *Australian Journal of Earth Sciences*, *48*(2), 265–280. http://doi.org/10.1046/j.1440-0952.2001.00858.x
Betts, P. G., Lister, G. S., & O'Dea, M. G. (1998). Asymmetric extension of the Middle Proterozoic lithosphere, Mount Isa terrane, Queensland, Australia. *Tectonophysics*, *296*(3–4), 293–316. http://doi.org/10.1016/s0040-1951(98)00144-9
Bierlein, F., Black, L., Hergt, J., & Mark, G. (2008). Evolution of Pre-1.8Ga basement rocks in the western Mt Isa Inlier, northeastern Australia—Insights from SHRIMP U-Pb dating and in-situ Lu-Hf analysis of zircons. *Precambrian Research*, *163*(1–2), 159–173. http://doi.org/10.1016/j.precamres.2007.08.017
Bird, P. (1979). Continental delamination and the Colorado Plateau. *Journal of Geophysical Research*, *84*(B13), 7561–7571. http://doi.org/10.1029/JB084iB13p07561
Blaikie, T. N., Betts, P. G., Armit, R. J., & Ailleres, L. (2017). The ca. 1740–1710 Ma Leichhardt Event: Inversion of a continental rift and revision of the tectonic evolution of the North Australian Craton. *Precambrian Research*, *292*, 75–92. http://doi.org/10.1016/j.precamres.2017.02.003
Blake, D. H. (1987). *Geology of the Mount Isa Inlier and environs, Queensland and Northern Territory* (Vol. 225). Australia: Bulletin - Bureau of Mineral Resources, Geology & Geophysics.
Blenkinsop, T. G. (2005). Total systems analysis of the Mount Isa eastern succession. Report. Predictive Mineral Discovery CRC.
Blenkinsop, T. G., Huddlestone-Holmes, C. R., Foster, D. R. W., Edmiston, M. A., Lepong, P., Mark, G., et al. (2008). The crustal scale architecture of the Eastern Succession, Mount Isa: The influence of inversion. *Precambrian Research*, *163*(1–2), 31–49. http://doi.org/10.1016/j.precamres.2007.08.011
Brown, M. (2007). Metamorphic conditions in orogenic belts: A record of secular change. *International Geology Review*, *49*(3), 193–234. http://doi.org/10.2747/0020-6814.49.3.193
Connors, K. A., & Lister, G. S. (1995). Polyphase deformation in the western Mount Isa Inlier, Australia: Episodic or continuous deformation? *Journal of Structural Geology*, *17*(3), 305–328.
Connors, K. A., & Page, R. W. (1995). Relationships between magmatism, metamorphism and deformation in the western Mount Isa Inlier. *Australia, Precambrian Research*, *71*(1–4), 131–153.
Day, R. W., Whitaker, W. G., Murray, C. G., Wilson, I. H., & Grimes, K. G. (1983). Queensland geology. A companion volume to the 1:2 500000 scale geological map (1975). *Geological Survey of Queensland*, *383*.
Derrick, G. (1982). A Proterozoic rift-zone at Mount-Isa, Queensland, and implications for mineralization. *BMR Journal of Australian Geology & Geophysics*, *7*(2), 81–92.
Dodson, M. H. (1973). Closure temperature in cooling geochronological and petrological systems. *Contributions to Mineralogy and Petrology*, *40*(3), 259–274. http://doi.org/10.1007/BF00373790
Duncan, R. J., Wilde, A. R., Bassano, K., & Maas, R. (2006). Geochronological constraints on tourmaline formation in the Western Fold Belt of the Mount Isa Inlier, Australia: Evidence for large-scale metamorphism at 1.57 Ga? *Precambrian Research*, *146*(3–4), 120–137. http://doi.org/10.1016/j.precamres.2006.01.010
Dunlap, W. J. (2000). Nature's diffusion experiment: The cooling-rate cooling-age correlation. *Geology*, *28*(2), 139–142.
England, P., & Houseman, G. (1989). Extension during continental convergence, with application to the Tibetan Plateau. *Journal of Geophysical Research*, *94*(B12), 17,561–17,579. http://doi.org/10.1029/JB094iB12p17561
Eriksson, K., Simpson, E., & Jackson, M. (1994). Stratigraphical evolution of a Proterozoic syn-rift to post-rift Basin: Constraints on the nature of lithospheric extension in the Mount Isa Inlier, Australia. *Tectonic Controls and Signatures in Sedimentary Successions*, 203–221. https://doi.org/10.1002/9781444304053.ch12
Etheridge, M. A., Rutland, R. W. R., & Wyborn, L. A. I. (1987). Orogenesis and tectonic process in the early to middle Proterozoic of northern Australia. *Precambrian Lithospheric Evolution*, *17*, 131–147.
Evans, D. A. D., & Mitchell, R. N. (2011). Assembly and breakup of the core of Paleoproterozoic-Mesoproterozoic supercontinent Nuna. *Geology*, *39*(5), 443–446. http://doi.org/10.1130/g31654.1
Evans, D. A. D., Veselovsky, R. V., Petrov, P. Y., Shatsillo, A. V., & Pavlov, V. E. (2016). Paleomagnetism of Mesoproterozoic margins of the Anabar Shield: A hypothesized billion-year partnership of Siberia and northern Laurentia. *Precambrian Research*, *281*, 639–655. http://doi.org/10.1016/j.precamres.2016.06.017
Foster, D. (2003). Proterozoic low-pressure metamorphism in the Mount Isa Inlier, northwest Queensland, Australia, with particular emphasis on the use of calcic amphibole chemistry as temperature-pressure indicators, *PhD thesis James Cook University*.
Foster, D., & Austin, J. (2008). The 1800–1610 Ma stratigraphic and magmatic history of the Eastern Succession, Mount Isa Inlier, and correlations with adjacent Paleoproterozoic terranes. *Precambrian Research*, *163*(1–2), 7–30. http://doi.org/10.1016/j.precamres.2007.08.010
Foster, D., & Rubenach, M. (2000). High radiogenic heat-producing granites and metamorphism—An example from the western Mount Isainlier, Australia: Comment. *Geology*, *28*(7), 671. http://doi.org/10.1130/0091-7613(2000)28<671:HRHGAM>2.0.CO;2

Foster, D. R. W., & Rubenach, M. J. (2006). Isograd pattern and regional low-pressure, high-temperature metamorphism of pelitic, mafic and calc-silicate rocks along an east-west section through the Mt Isa Inlier. *Australian Journal of Earth Sciences*, *53*(1), 167–186. http://doi.org/10.1080/08120090500434617

Furlanetto, F., Thorkelson, D. J., Daniel Gibson, H., Marshall, D. D., Rainbird, R. H., Davis, W. J., et al. (2013). Late Paleoproterozoic terrane accretion in northwestern Canada and the case for circum-Columbian orogenesis. *Precambrian Research*, *224*, 512–528. http://doi.org/10.1016/j.precamres.2012.10.010

Gauthier, L., Hall, G., Stein, H., & Schaltegger, U. (2001). The Osborne deposit, Cloncurry district: A 1595 Ma Cu-Au skarn deposit. *A Hydrothermal Odyssey, New Developments in Metalliferous Hydrothermal Systems Research*, *59*, 58–59.

Gibson, G. M., Champion, D. C., Withnall, I. W., Neumann, N. L., & Hutton, L. J. (2018). Assembly and breakup of the Nuna supercontinent: Geodynamic constraints from 1800 to 1600 Ma sedimentary basins and basaltic magmatism in northern Australia. *Precambrian Research*, *313*, 148–169. http://doi.org/10.1016/j.precamres.2018.05.013

Gibson, G. M., Henson, P. A., Neumann, N. L., Southgate, P. N., & Hutton, L. J. (2012). Paleoproterozoic-earliest Mesoproterozoic basin evolution in the Mount Isa region, northern Australia and implications for reconstructions of the Nuna and Rodinia supercontinents. *Episodes*, *35*(1), 131–141.

Gibson, G. M., Rubenach, M. J., Neumann, N. L., Southgate, P. N., & Hutton, L. J. (2008). Syn- and post-extensional tectonic activity in the Palaeoproterozoic sequences of Broken Hill and Mount Isa and its bearing on reconstructions of Rodinia. *Precambrian Research*, *166*(1–4), 350–369. http://doi.org/10.1016/j.precamres.2007.05.005

Giles, D., Ailléres, L., Jeffries, D., Betts, P., & Lister, G. (2006). Crustal architecture of basin inversion during the Proterozoic Isan Orogeny, Eastern Mount Isa Inlier, Australia. *Precambrian Research*, *148*(1–2), 67–84. http://doi.org/10.1016/j.precamres.2006.03.002

Giles, D., & Nutman, A. P. (2002). SHRIMP U-Pb monazite dating of 1600–1580 Ma amphibolite facies metamorphism in the southeastern Mt Isa Block, Australia. *Australian Journal of Earth Sciences*, *49*(3), 455–465. http://doi.org/10.1046/j.1440-0952.2002.00931.x

Grove, M., & Harrison, T. M. (1996). ^{40}Ar* diffusion in Fe-rich biotite. *American Mineralogist*, *81*(7–8), 940–951. http://doi.org/10.2138/am-1996-7-816

Hand, M., & Rubatto, D. (2002). The scale of the thermal problem in the Mount Isa Inlier, Geological Society of Australia Abstracts, *67*.

Hansma, J., Tohver, E., Schrank, C., Jourdan, F., & Adams, D. (2016). The timing of the Cape Orogeny: New ^{40}Ar/^{39}Ar age constraints on deformation and cooling of the Cape Fold Belt, South Africa. *Gondwana Research*, *32*, 122–137. http://doi.org/10.1016/j.gr.2015.02.005

Harrison, T. M. (1981). Diffusion of ^{40}Ar in hornblende. *Contributions to Mineralogy & Petrology*, *78*(3), 324–331.

Harrison, T. M., Célérier, J., Aikman, A. B., Hermann, J., & Heizler, M. T. (2009). Diffusion of ^{40}Ar in muscovite. *Geochimica et Cosmochimica Acta*, *73*(4), 1039–1051. http://doi.org/10.1016/j.gca.2008.09.038

Harrison, T. M., Duncan, I., & McDougall, I. (1985). Diffusion of ^{40}Ar in biotite: Temperature pressure and compositional effects. *Geochimica et Cosmochimica Acta*, *49*(11), 2461–2468. http://doi.org/10.1016/0016-7037(85)90246-7

Holcombe, R. J., Pearson, P. J., & Oliver, N. H. S. (1991). Geometry of a Middle Proterozoic extensional décollement in northeastern Australia. *Tectonophysics*, *191*(3–4), 255–274. http://doi.org/10.1016/0040-1951(91)90061-V

Jackson, M. J., Scott, D. L., & Rawlings, D. J. (2000). Stratigraphic framework for the Leichhardt and Calvert Superbasins: Review and correlations of the pre-1700 Ma successions between Mt Isa and McArthur River. *Australian Journal of Earth Sciences*, *47*(3), 381–403. http://doi.org/10.1046/j.1440-0952.2000.00789.x

Jackson, M. J., & Southgate, P. N. (2000). Evolution of three unconformity-bounded sandy carbonate successions in the McArthur River region of northern Australia: The Lawn, Wide and Doom Supersequences in a proximal part of the Isa Superbasin. *Australian Journal of Earth Sciences*, *47*(3), 625–635. http://doi.org/10.1046/j.1440-0952.2000.00786.x

Jamieson, R. A., & Beaumont, C. (2013). On the origin of orogens. *Geological Society of America Bulletin*, *125*(11–12), 1671–1702. https://doi.org/10.1130/b30855.1

Jamieson, R. A., Beaumont, C., Nguyen, M. H., & Lee, B. (2002). Interaction of metamorphism, deformation and exhumation in large convergent orogens. *Journal of Metamorphic Geology*, *20*(1), 9–24. https://doi.org/10.1046/j.0263-4929.2001.00357.x

Jiménez-Munt, I., Fernàndez, M., Vergés, J., & Platt, J. P. (2008). Lithosphere structure underneath the Tibetan Plateau inferred from elevation, gravity and geoid anomalies. *Earth and Planetary Science Letters*, *267*(1–2), 276–289. http://doi.org/10.1016/j.epsl.2007.11.045

Johnson, M. R., Harley, S. L., & Harley, S. (2012). *Orogenesis: The making of mountains*. Cambridge, UK: Cambridge University Press.

Kearey, P., Klepeis, K. A., & Vine, F. J. (2009). *Global tectonics*. West Sussex, UK: John Wiley & Sons.

Kelley, S. (2002). Excess argon in K-Ar and Ar-Ar geochronology. *Chemical Geology*, *188*(1–2), 1–22.

Kirscher, U., Liu, Y., Li, Z. X., Mitchell, R. N., Pisarevsky, S. A., Denyszyn, S. W., & Nordsvan, A. (2019). Paleomagnetism of the Hart Dolerite (Kimberley, Western Australia)—A two-stage assembly of the supercontinent Nuna? *Precambrian Research*, *329*, 170–181. http://doi.org/10.1016/j.precamres.2018.12.026

Kirscher, U., Mitchell, R. N., Liu, Y., Nordsvan, A. R., Cox, G. M., Pisarevsky, S. A., et al. (2020). Paleomagnetic constraints on the duration of the Australia-Laurentia connection in the core of the Nuna supercontinent. *Geology*. https://doi.org/10.1130/G47823.1

Korja, A., Kosunen, P., & Heikkinen, P. (2009). A case study of lateral spreading: the Precambrian Svecofennian Orogen. *Geological Society, London, Special Publications*, *321*(1), 225–251. https://doi.org/10.1144/sp321.11

Li, Z. X., Li, X. H., Wartho, J. A., Clark, C., Li, W. X., Zhang, C. L., & Bao, C. M. (2010). Magmatic and metamorphic events during the early Paleozoic Wuyi-Yunkai orogeny, southeastern South China: New age constraints and pressure-temperature conditions. *Geological Society of America Bulletin*, *122*, 772–793.

Lister, G. S., O'Dea, M. G., & Somaia, I. (1999). A tale of two synclines: Rifting, inversion and transpressional popouts at Lake Julius, northwestern Mt Isa terrane, Queensland. *Australian Journal of Earth Sciences*, *46*(2), 233–250. http://doi.org/10.1046/j.1440-0952.1999.00690.x

Loosveld, R. J. H. (1989). The synchronism of crustal thickening and high T/low P metamorphism in the Mount Isa Inlier, Australia 1. An example, the central Soldiers Cap belt. *Tectonophysics*, *158*(1–4), 173–190. http://doi.org/10.1016/0040-1951(89)90323-5

MacCready, T. (2006). Structural cross-section based on the Mt Isa deep seismic transect. *Australian Journal of Earth Sciences*, *53*(1), 5–26. http://doi.org/10.1080/08120090500431415

Maccready, T., Goleby, B. R., Goncharov, A., Drummond, B. J., & Lister, G. S. (1998). A framework of overprinting orogens based on interpretation of the Mount Isa deep seismic transect. *Economic Geology*, *93*(8), 1422–1434. http://doi.org/10.2113/gsecongeo.93.8.1422

Mark, G. (2001). Nd isotope and petrogenetic constraints for the origin of the Mount Angelay igneous complex: Implications for the origin of intrusions in the Cloncurry district, NE Australia. *Precambrian Research*, *105*(1), 17–35. http://doi.org/10.1016/s0301-9268(00)00101-7

McConachie, B., Barlow, M., Dunster, J., Meaney, R., & Schaap, A. (1993). The Mount Isa Basin—Definition, structure and petroleum geology. *The APPEA Journal*, *33*(1), 237–257.

McDonald, C. S., Regis, D., Warren, C. J., Kelley, S. P., & Sherlock, S. C. (2018). Recycling argon through metamorphic reactions: The record in symplectites. *Lithos*, *300-301*, 200–211. http://doi.org/10.1016/j.lithos.2017.11.028

McDougall, I., & Harrison, T. M. (1999). *Geochronology and thermochronology by the $^{40}Ar/^{39}Ar$ method*. Oxford, UK: Oxford University Press on Demand.

McLaren, S., Sandiford, M., & Hand, M. (1999). High radiogenic heat–producing granites and metamorphism—An example from the western Mount Isa inlier, Australia. *Geology*, *27*(8), 679–682. https://doi.org/10.1130/0091-7613(1999)027<0679:hrhpga>2.3.co;2

McLaren, S., Sandiford, M., & Powell, R. (2005). Contrasting styles of Proterozoic crustal evolution: A hot-plate tectonic model for Australian terranes. *Geology*, *33*(8), 673. https://doi.org/10.1130/g21544.1

Meng, L., Li, Z.-X., Chen, H., Li, X.-H., & Wang, X.-C. (2012). Geochronological and geochemical results from Mesozoic basalts in southern South China Block support the flat-slab subduction model. *Lithos*, *132*, 127–140.

Montgomery, D. R., & Brandon, M. T. (2002). Topographic controls on erosion rates in tectonically active mountain ranges. *Earth and Planetary Science Letters*, *201*(3–4), 481–489. https://doi.org/10.1016/S0012-821X(02)00725-2

Neumann, N. L., Gibson, G. M., & Southgate, P. N. (2009). New SHRIMP age constraints on the timing and duration of magmatism and sedimentation in the Mary Kathleen Fold Belt, Mt Isa Inlier, Australia. *Australian Journal of Earth Sciences*, *56*(7), 965–983. http://doi.org/10.1080/08120090903005410

Neumann, N. L., Southgate, P. N., Gibson, G. M., & McIntyre, A. (2006). New SHRIMP geochronology for the Western Fold Belt of the Mt Isa Inlier: Developing a 1800–1650 Ma event framework. *Australian Journal of Earth Sciences*, *53*(6), 1023–1039. http://doi.org/10.1080/08120090600923287

Nordsvan, A. R., Collins, W. J., & Li, Z.-X. (2018). A piece of North America is now in Queensland. *Australian Science*, *39*(3), 17.

Nordsvan, A. R., Collins, W. J., Li, Z.-X., Spencer, C. J., Pourteau, A., Withnall, I. W., et al. (2018). Laurentian crust in northeast Australia: Implications for the assembly of the supercontinent Nuna. *Geology*, *46*(3), 251–254. http://doi.org/10.1130/g39980.1

O'Dea, M. G., Lister, G. S., Maccready, T., Betts, P. G., Oliver, N. H. S., Pound, K. S., et al. (1997). Geodynamic evolution of the Proterozoic Mount Isa terrain. *Geological Society, London, Special Publications*, *121*(1), 99–122. http://doi.org/10.1144/gsl.sp.1997.121.01.05

O'Dea, M. G., Betts, P. G., MacCready, T., & Aillères, L. (2006). Sequential development of a mid-crustal fold-thrust complex: Evidence from the Mitakoodi Culminationin the eastern Mt Isa Inlier, Australia. *Australian Journal of Earth Sciences*, *53*(1), 69–90. http://doi.org/10.1080/08120090500432447

O'Dea, M. G., & Lister, G. S. (1995). The role of ductility contrast and basement architecture in the structural evolution of the Crystal Creek block, Mount Isa Inlier, NW Queensland, Australia. *Journal of Structural Geology*, *17*(7), 949–960. http://doi.org/10.1016/0191-8141(94)00117-I

O'Dea, M. G., Lister, G. S., Betts, P. G., & Pound, K. S. (1997). A shortened intraplate rift system in the Proterozoic Mount Isa terrane, NW Queensland, Australia. *Tectonics*, *16*(3), 425–441. http://doi.org/10.1029/96TC03276

Oliver, N. H., Holcombe, R. J., Hill, E. J., & Pearson, P. J. (1991). Tectono-metamorphic evolution of the Mary Kathleen Fold Belt, northwest Queensland: A reflection of mantle plume processes? *Australian Journal of Earth Sciences*, *38*(4), 425–455. http://doi.org/10.1080/08120099108727982

Page, R., Sun, S., & MacCready, T. (1997). New geochronological results in the central and eastern Mount Isa Inlier and implications for mineral exploration, paper presented at Geodynamics and Ore Deposits Conference Abstracts, Australian Geodynamics Cooperative Research Centre.

Page, R. W. (1983). Chronology of magmatism, skarn formation, and uranium mineralization, Mary-Kathleen, Queensland, Australia. *Economic Geology*, *78*(5), 838–853. http://doi.org/10.2113/gsecongeo.78.5.838

Page, R. W. (1998). Links between Eastern and Western fold belts in the Mount Isa Inlier, based on SHRIMP U-Pb studies. *Geological Society of Australia Abstracts*, *49*, 349.

Page, R. W., & Bell, T. H. (1986). Isotopic and structural responses of granite to successive deformation and metamorphism. *The Journal of Geology*, *94*(3), 365–379. http://doi.org/10.1086/629035

Page, R. W., & Sun, S. S. (1998). Aspects of geochronology and crustal evolution in the Eastern Fold Belt, Mt Isa Inlier. *Australian Journal of Earth Sciences*, *45*(3), 343–361. http://doi.org/10.1080/08120099808728396

Page, R. W., & Williams, I. (1988). Age of the Barramundi Orogeny in northern Australia by means of ion microprobe and conventional U-Pb zircon studies. *Precambrian Research*, *40*, 21–36.

Pearson, P. (1992). Synkinematic emplacement of the Middle Proterozoic Wonga batholith into a midcrustal extensional shear zone, Mount Isa Inlier, Queensland, Australia. *Detailed Studies of the Mount Isa Inlier*, 289–328. https://ci.nii.ac.jp/naid/10027157550/

Pehrsson, S. J., Eglington, B. M., Evans, D. A. D., Huston, D., & Reddy, S. M. (2016). Metallogeny and its link to orogenic style during the Nuna supercontinent cycle. *Geological Society, London, Special Publications*, *424*(1), 83–94. http://doi.org/10.1144/sp424.5

Perkins, C., Heinrich, C. A., & Wyborn, L. A. (1999). $^{40}Ar/^{39}Ar$ geochronology of copper mineralization and regional alteration, Mount Isa, Australia. *Economic Geology*, *94*(1), 23–36.

Perkins, C., & Wyborn, L. A. I. (1998). Age of Cu-Au mineralisation, Cloncurry district, eastern Mt Isa Inlier, Queensland, as determined by $^{40}Ar/^{39}Ar$ dating. *Australian Journal of Earth Sciences*, *45*(2), 233–246. https://doi.org/10.1080/08120099808728384

Pinet, P., & Souriau, M. (1988). Continental erosion and large-scale relief. *Tectonics*, *7*(3), 563–582. https://doi.org/10.1029/TC007i003p00563

Pisarevsky, S. A., Elming, S.-A., Pesonen, L. J., & Li, Z.-X. (2014). Mesoproterozoic paleogeography: Supercontinent and beyond. *Precambrian Research*, *244*, 207–225. http://doi.org/10.1016/j.precamres.2013.05.014

Pollard, P., & McNaughton, N. (1997). U/Pb geochronology and Sm/Nd isotope characterization of Proterozoic intrusive rocks in the Cloncurry district, Mount Isa inlier, Australia, *AMIRA P438 Cloncurry Base Metals and Gold Final Report*. *Section*, *4*, 19.

Pollard, P., & Perkins, C. (1997). $^{40}Ar/^{39}Ar$ geochronology of alteration and Cu-Au-Co mineralization in the Cloncurry district, Mount Isa Inlier, Australia, *AMIRA P438 Cloncurry Base Metals and Gold Final Report*.

Pollard, P. J., Mark, G., & Mitchell, L. C. (1998). Geochemistry of post-1540 Ma granites in the Cloncurry district, northwest Queensland. *Economic Geology and the Bulletin of the Society of Economic Geologists*, *93*(8), 1330–1344. http://doi.org/10.2113/gsecongeo.93.8.1330

Pourteau, A., Smit, M. A., Li, Z.-X., Collins, W. J., Nordsvan, A. R., Volante, S., & Li, J. (2018). 1.6 Ga crustal thickening along the final Nuna suture. *Geology*, *46*(11), 959–962.

Reinhardt, J. (1992a). The Corella Formation of the Rosebud Syncline (central Mount Isa Inlier): Deposition, deformation, and metamorphism, Detailed studies of the Mount Isa Inlier, 229–255.

Reinhardt, J. (1992b). Low-pressure, high-temperature metamorphism in a compressional tectonic setting: Mary Kathleen Fold Belt, northeastern Australia. *Geological Magazine*, *129*(1), 41–57. http://doi.org/10.1017/S0016756800008116

Renne, P. R., Balco, G., Ludwig, K. R., Mundil, R., & Min, K. (2011). Response to the comment by W.H. Schwarz et al. on "Joint determination of ^{40}K decay constants and ^{40}Ar*/^{40}K for the Fish Canyon sanidine standard, and improved accuracy for ^{40}Ar/^{39}Ar geochronology" by PR Renne et al. (2010). *Geochimica et Cosmochimica Acta*, *75*(17), 5097–5100. http://doi.org/10.1016/j.gca.2011.06.021

Richards, J. R., Cooper, J. A., & Webb, A. W. (1963). Potassium-argon ages on micas from the Precambrian region of North-Western Queensland. *Journal of the Geological Society of Australia*, *10*(2), 299–312. http://doi.org/10.1080/00167616308728547

Rivers, T. (2012). Upper-crustal orogenic lid and mid-crustal core complexes: signature of a collapsed orogenic plateau in the hinterland of the Grenville Province 1This article is one of a series of papers published in CJES Special Issue: In honour of Ward Neale on the theme of Appalachian and Grenvillian geology. *Canadian Journal of Earth Sciences*, *49*(1), 1–42. https://doi.org/10.1139/e11-014

Rogers, J. J. W., & Santosh, M. (2002). Configuration of Columbia, a mesoproterozoic supercontinent. *Gondwana Research*, *5*(1), 5–22. http://doi.org/10.1016/s1342-937x(05)70883-2

Rubenach, M. J. (1992). Proterozoic low-pressure/high-temperature metamorphism and an anticlockwise P-T-t path for the Hazeldene area, Mount Isa Inlier, Queensland, Australia. *Journal of Metamorphic Geology*, *10*(3), 333–346. http://doi.org/10.1111/j.1525-1314.1992.tb00088.x

Rubenach, M. J., & Barker, A. J. (1998). Metamorphic and metasomatic evolution of the Snake Creek Anticline, Eastern Succession, Mt Isa Inlier. *Australian Journal of Earth Sciences*, *45*(3), 363–372. http://doi.org/10.1080/08120099808728397

Rubenach, M. J., Foster, D. R. W., Evins, P. M., Blake, K. L., & Fanning, C. M. (2008). Age constraints on the tectonothermal evolution of the Selwyn Zone, Eastern Fold Belt, Mount Isa Inlier. *Precambrian Research*, *163*(1–2), 81–107. http://doi.org/10.1016/j.precamres.2007.08.014

Rubenach, M. J., & Lewthwaite, K. A. (2002). Metasomatic albitites and related biotite-rich schists from a low-pressure polymetamorphic terrane, Snake Creek Anticline, Mount Isa Inlier, north-eastern Australia: Microstructures and P-T-d paths. *Journal of Metamorphic Geology*, *20*(1), 191–202. http://doi.org/10.1046/j.0263-4929.2001.00348.x

Rubio Pascual, F. J., Arenas, R., Martínez Catalán, J. R., Rodríguez Fernández, L. R., & Wijbrans, J. R. (2013). Thickening and exhumation of the Variscan roots in the Iberian Central System: Tectonothermal processes and 40Ar/39Ar ages. *Tectonophysics*, *587*, 207–221. https://doi.org/10.1016/j.tecto.2012.10.005

Sayab, M. (2006). Decompression through clockwise P-T path: Implications for early N-S shortening orogenesis in the Mesoproterozoic Mt Isa Inlier (NE Australia). *Journal of Metamorphic Geology*. http://doi.org/10.1111/j.1525-1314.2006.00626.x

Sayab, M. (2009). Tectonic significance of structural successions preserved within low-strain pods: Implications for thin- to thick-skinned tectonics vs. multiple near-orthogonal folding events in the Palaeo-Mesoproterozoic Mount Isa Inlier (NE Australia). *Precambrian Research*, *175*(1–4), 169–186. http://doi.org/10.1016/j.precamres.2009.09.007

Scibiorski, E., Tohver, E., & Jourdan, F. (2015). Rapid cooling and exhumation in the western part of the Mesoproterozoic Albany-Fraser Orogen, Western Australia. *Precambrian Research*, *265*, 232–248. http://doi.org/10.1016/j.precamres.2015.02.005

Schulmann, K., Lexa, O., Štípská, P., Racek, M., Tajčmanová, L., Konopásek, J., et al. (2008). Vertical extrusion and horizontal channel flow of orogenic lower crust: key exhumation mechanisms in large hot orogens? *Journal of Metamorphic Geology*, *26*(2), 273–297. https://doi.org/10.1111/j.1525-1314.2007.00755.x

Skipton, D. R., Schneider, D. A., Kellett, D. A., & Joyce, N. L. (2017). Deciphering the Paleoproterozoic cooling history of the northeastern Trans-Hudson Orogen, Baffin Island (Canada), using ^{40}Ar/^{39}Ar step-heating and UV laser thermochronology. *Lithos*, *284*, 69–90. http://doi.org/10.1016/j.lithos.2017.03.023

Southgate, P. N., Neumann, N. L., & Gibson, G. M. (2013). Depositional systems in the Mt Isa Inlier from 1800 Ma to 1640 Ma: Implications for Zn-Pb-Ag mineralisation. *Australian Journal of Earth Sciences*, *60*(2), 157–173. http://doi.org/10.1080/08120099.2013.758176

Southgate, P. N., Scott, D. L., Sami, T. T., Domagala, J., Jackson, M. J., James, N. P., & Kyser, T. K. (2000). Basin shape and sediment architecture in the Gun Supersequence: A strike-slip model for Pb-Zn-Ag ore genesis at Mt Isa. *Australian Journal of Earth Sciences*, *47*(3), 509–531. http://doi.org/10.1046/j.1440-0952.2000.00792.x

Spikings, R. A., Foster, D. A., & Kohn, B. P. (1997). Phanerozoic denudation history of the Mount Isa Inlier, Northern Australia: Response of a Proterozoic mobile belt to intraplate tectonics. *International Geology Review*, *39*(2), 107–124. http://doi.org/10.1080/00206819709465262

Spikings, R. A., Foster, D. A., Kohn, B. P., & Lister, G. S. (2001). Post-orogenic (<1500 Ma) thermal history of the Proterozoic Eastern Fold Belt, Mount Isa Inlier, Australia. *Precambrian Research*, *109*(1–2), 103–144. http://doi.org/10.1016/s0301-9268(01)00143-7

Spikings, R. A., Foster, D. A., Kohn, B. P., & Lister, G. S. (2002). Post-orogenic (<1500 Ma) thermal history of the Palaeo-Mesoproterozoic, Mt Isa province, NE Australia. *Tectonophysics*, *349*(1–4), 327–365. http://doi.org/10.1016/s0040-1951(02)00060-4

Stübner, K., Grujic, D., Dunkl, I., Thiede, R., & Eugster, P. (2018). Pliocene episodic exhumation and the significance of the Munsiari thrust in the northwestern Himalaya. *Earth and Planetary Science Letters*, *481*, 273–283.

Thorkelson, D. J., Abbott, J. A., Mortensen, J. K., Creaser, R. A., Villeneuve, M. E., McNicoll, V. J., & Layer, P. W. (2005). Early and Middle Proterozoic evolution of Yukon, Canada. *Canadian Journal of Earth Sciences*, *42*(6), 1045–1071. http://doi.org/10.1139/e05-075

Volante, S., Collins, W. J., Pourteau, A., Li, Z. X., Li, J., & Nordsvan, A. R. (2020). Structural evolution of a 1.6 Ga orogeny related to the final assembly of the supercontinent Nuna: Coupling of episodic and progressive deformation. *Tectonics*, *39*, e2020TC006162. https://doi.org/10.1029/2020TC006162

Volante, S., Pourteau, A., Collins, W. J., Blereau, E., Li, Z.-X., Smit, M., et al. (2020). Multiple P-T-d-t paths reveal the evolution of the final Nuna assembly in northeast Australia. *Journal of Metamorphic Geology*, *38*(6), 593–627. https://doi.org/10.1111/jmg.12532

Warren, C. J., Kelley, S. P., Sherlock, S. C., & McDonald, C. S. (2012). Metamorphic rocks seek meaningful cooling rate: Interpreting 40Ar/39Ar ages in an exhumed ultra-high pressure terrane. *Lithos*, *155*, 30–48. https://doi.org/10.1016/j.lithos.2012.08.011

White, W. M. (2013). *Geochemistry*. West Sussex, UK: John Wiley & Sons.

Williams, P. J., & Phillips, G. N. (1992). Cloncurry mapping project 1990: Geology of the Selwyn Range (McKinlay River and Maramungee Creek areas), *Contributions - James Cook University*, Economic Geology Research Unit, 40.

Withnall, I. W., & Hutton, L. J. (2013). Proterozoic-North Australian Craton, Geology of Queensland, 23–112.

Wyborn, L. (1998). Younger ca 1500 Ma granites of the Williams and Naraku Batholiths, Cloncurry district, eastern Mt Isa Inlier: Geochemistry, origin, metallogenic significance and exploration indicators. *Australian Journal of Earth Sciences*, *45*(3), 397–411. http://doi.org/10.1080/08120099808728400

Yao, W.-H., Li, Z.-X., Li, W.-X., Wang, X.-C., Li, X.-H., & Yang, J.-H. (2012). Post-kinematic lithospheric delamination of the Wuyi-Yunkai orogen in South China: Evidence from ca. 435 Ma high-Mg basalts. *Lithos*, *154*, 115–129. http://doi.org/10.1016/j.lithos.2012.06.033

Zhang, S., Li, Z.-X., Evans, D. A. D., Wu, H., Li, H., & Dong, J. (2012). Pre-Rodinia supercontinent Nuna shaping up: A global synthesis with new paleomagnetic results from North China. *Earth and Planetary Science Letters*, *353–354*, 145–155. http://doi.org/10.1016/j.epsl.2012.07.034

Zhao, G., Cawood, P. A., Wilde, S. A., & Sun, M. (2002). Review of global 2.1–1.8 Ga orogens: Implications for a pre-Rodinia supercontinent. *Earth-Science Reviews*, *59*(1–4), 125–162. http://doi.org/10.1016/s0012-8252(02)00073-9